Continuous Analogs of Digital Boundaries: A Topological Approach to Iso-Surfaces

Jacques-Olivier Lachaud[1] and Annick Montanvert[2]

[1] Laboratoire Bordelais de Recherche en Informatique
Domaine Universitaire
351 Cours de la Libération
33405 Talence, France
e-mail: lachaud@labri.u-bordeaux.fr
phone: +33-(0)5.56.84.69.12

[2] Laboratoire des Images et des Signaux
961 rue de la Houille Blanche
Domaine Universitaire, BP 46
38402 Saint Martin d'Hères cedex, France
e-mail: annick.montanvert@inpg.fr
phone: +33-(0)4.76.82.64.67

Abstract:

The definition and extraction of objects and their boundaries within an image are essential in many imaging applications. Classically, two approaches are followed. The first considers the image as a sample of a continuous scalar field: boundaries are implicit surfaces in this field; they are often called *iso-surfaces*. The second considers the image as a digital space with adjacency relations and classifies elements of this space as inside or outside: boundaries are pairs composed of one inside element and one outside element; they are called *digital boundaries*. In this paper, we show that these two approaches are closely related. This statement holds for arbitrary dimensions. To do so, we propose a local method to construct a *continuous analog* of a digital boundary. The continuous analog is designed to satisfy properties in the Euclidean space that are similar to the properties of its counterpart in the digital space (e.g., connectedness, closeness, separation). It appears that this continuous analog is indeed a piecewise linear approximation of an iso-(hyper)surface (i.e., a triangulated iso-surface in the three-dimensional case). Furthermore, we derive significant digital boundary properties from its continuous analog using the Jordan–Brouwer separation theorem: new *Jordan pairs*, new adjacencies between boundary elements, new *Jordan triples*. We conclude this paper by illustrating the 3D case more precisely. In particular, we show that a digital boundary can be transformed directly into a triangulated iso-surface. The implementation of this transformation and its efficiency are discussed with a comparison with the classical *marching-cubes* algorithm.

1 Introduction

In many areas of science and engineering, n-dimensional (nD) data sets representing a sample of some physical phenomenon at discrete locations (e.g., in space, in time) are routinely produced. With a careful study of these samples, it is possible to extract valuable information on the characteristics of the analyzed objects. When a sample is taken on the vertices of a discrete grid and is scalar valued, the term *image* is often employed. Many imaging applications need to define and extract boundaries of objects from these images, for instance for visualization, shape recovery, quantitative analysis, editing, or simulation. The induced issues have been tackled in many ways (e.g., surface and volume rendering, deformable models, reconstruction from slices, level-set approaches), but discrete methods for extracting boundaries (i.e., surfaces in the 3D case) have appeared to be a good (and fast) trade-off for this purpose. Although 2D and 3D images are currently the most common images, higher dimensional images are now available and are likely to become more common in the near future. Dynamic magnetic resonance images (cardiac imagery) and spectroscopic magnetic resonance images are examples of 4D images. Five dimensional images have also been reported in the literature [13].

Two classes of discrete methods have been used to tackle the boundary extraction problem. One embeds the image into the Euclidean space to extract triangulated (hyper)-surfaces in this space, the image discreteness providing the resolution of the reconstruction. The other considers the image as a digital space and extracts digital boundaries. In a final phase, the digital boundaries can be immersed in the space as a set of squares or rectangular elements (in 3D), e.g., for visualization purposes. Even if many algorithms found in the literature are 3D, arbitrary dimensional methods to extract boundaries are available, both in the continuous point of view [4] and in the digital point of view [41]).

The methods of the first class consider the image as a sampling of a scalar continuous field on the points of a discrete grid. Their objective is to extract a piecewise linear approximation of an implicitly defined surface inside this field (i.e., a triangulated surface in the 3D case). Since the implicit surface is defined as a set of points having the same value in the field, these methods are often called *iso-surface extraction* methods. The extracted triangulated surfaces delineate boundaries of objects in the image. Note that many *implicit surface polygonization* methods, which are devoted to the *tiling* of implicit surfaces within an analytically defined field,

can be employed to extract iso-surfaces in most cases. Roughly speaking, these methods can be divided into two groups (a survey can be found in [8]): one group *scans* (either by regular, irregular or hierarchical subdivision of the space) the whole domain of the field to extract all the components of the implicitly defined surface [7, 9, 10, 12, 20, 30, 40, 44], the other group *tracks* one connected component of the implicitly defined surface [3, 4, 7, 45]. These methods construct triangulated surfaces that possess good topological and geometrical properties (manifolds in the space, piecewise linear surfaces), and they can be rendered efficiently on modern workstations. Furthermore, these surfaces can easily be reused in other applications (e.g., biomedical simulators, CAGD applications, computer assisted surgery) for visualization, analysis or editing.

The methods of the second class consider the image as a discrete space of points with a certain definition of adjacency between these points; these points are classically called *voxels*. They assume that a preprocessing step has classified these voxels as *foreground* voxels or *background* voxels. The *objects* inside the image are then defined as the connected component of foreground voxels determined by the adjacency. For visualization and analysis of these objects (especially if the dimension of the image is greater than or equal to two), it is more convenient and more efficient to use a boundary description of these objects in the form of a *digital boundary*. An important amount of literature has been devoted to their definitions in varied digital spaces and corresponding properties, and to their computation [5, 15, 19, 16, 18, 1, 17, 29, 24, 43, 41]. Digital boundaries have significant topological properties in the digital space (digital analog of Jordan property) and, to some extent, they can be used for quantitative analysis and object editing. Compared to triangulated iso-surfaces, connected digital boundaries may also represent an iso-surface approximation and are more quickly computed and displayed. However, their geometrical characteristics are less readily defined since they are classically embedded in the Euclidean space as orthogonal rectangular elements. Defining consistent geometrical characteristics to digital sets is currently an active area of research (which is generally called *discrete geometry*).

Although these two classes of approaches share the same objective, they are hardly ever related. Indeed, finding an iso-surface of value s inside a gray-level image is similar to finding the boundaries of the same image but thresholded by s. In this paper, we propose a local

approach to construct a *continuous analog* of any digital boundary in arbitrary dimension. The continuous analog may be seen as an *embedding into the Euclidean space* of a digital boundary, whose topology is dependent on the topology of the digital boundary (the chosen digital adjacencies), and whose geometry is dependent on an embedding function (similar to the linear interpolation of iso-surface extraction methods). By this way, continuous analogs share many common properties with their counterpart in the digital space: each continuous analog is (strongly) connected and disjoint from other continuous analogs of the image, two points separated by a digital boundary in the digital space are separated by its continuous analog in the Euclidean space and conversely, there is a one-to-one correspondence between the set of elements of a digital boundary and the set of vertices of its counterpart. The continuous analog is defined as a $(n-1)$-dimensional polyhedral complex with manifold properties. Using this definition, the following significant results are demonstrated in this paper:

- Continuous analogs are piecewise linear approximations of an iso-potential set (multidimensional extension of iso-surface) in a gray-level image. In the 3D space, we show that continuous analogs correspond nicely to triangulated iso-surfaces.
- New properties of digital boundaries are deduced from classical results of Euclidean space topology (especially the Jordan–Brouwer separation theorem): new *Jordan pairs* [16] and *Jordan triples* [41] are exhibited for arbitrary dimensions.
- In the 3D space, we show that a digital boundary along with the adjacencies between its elements is closely related to triangulated iso-surface as constructed by the *marching-cubes* algorithm [30] and its derivatives. Consequently, classical algorithms of digital surface tracking [5, 15] could be used to quickly construct a connected continuous analog, hence a component of the iso-surface.
- Contrary to other existing arbitrary dimensional methods which extract implicit (hyper)-surfaces with a simplicial decomposition of the space [4], our approach is based on a cubical decomposition of the space. A greater piece of the (hyper)-surface is thus built at each step.

This paper is organized as follows. In Section 2, we recall useful definitions of digital and combinatorial topology and we present how a set of voxels considered with an adjacency

relation can be mapped into the Euclidean space, so that they possess analog properties. In Section 3, we define the continuous analog of digital boundaries in arbitrary dimension and we exhibit several properties of these sets. In Section 4, different applications of continuous analogs are presented. Section 5 is devoted to the 3D case, where the relationship between digital boundaries and triangulated iso-surfaces is precisely examined. Section 6 states some concluding remarks. Appendices present the notation conventions used throughout the paper as well as several convex analytic geometry and combinatorial topology definitions and results.

2 Preliminary definitions

In this section, we recall useful definitions of digital topology and of combinatorial topology. After that, we propose a method to map voxels into the Euclidean space according to their adjacencies; i.e., we build a continuous analog of a set of voxels. *This mapping will be critical to deduce properties on digital boundaries in Section 4.* In order to have a continuous analog, a digital boundary must be defined by adjacencies that follow some properties: these properties are described at the end of this section.

2.1 Digital topology definitions

2.1.1 Voxel, image, binary image

In this paper, we assume that n is an integer number with $n \geq 2$. We will interpret $\mathbb{Z}^n$ as the set of points with integer coordinates in the Euclidean n-dimensional space $\mathbb{R}^n$. A *voxel* is an element of $\mathbb{Z}^n$; it is thus a point in $\mathbb{R}^n$ with integer coordinates. (Some authors [41] use the term "spel" for a voxel in a n-dimensional space; since we feel that no confusion should arise, we keep the term "voxel" for any dimension.) If u is a voxel of $\mathbb{Z}^n$, its i-th coordinate, $1 \leq i \leq n$, is denoted by $u^{(i)}$.

Let E be a "digital parallelepiped," i.e., $E = \{u \in \mathbb{Z}^n \mid -e^{(i)} \leq u^{(i)} \leq e^{(i)}\}$ for some voxel e in the strictly positive orthant of $\mathbb{Z}^n$. An *image* I on $\mathbb{Z}^n$ is a tuple (E, f) where f is a mapping from the subset E of $\mathbb{Z}^n$, called the *domain* of I, toward a set of numbers, called the *range* of I. An image whose range is $\{0, 1\}$ is called a *binary image*. The *value* of a voxel $u \in E$ in the image I is the number $f(u)$. The domain is finite by definition. Furthermore we consider only

images where all voxels on the border of the domain have the same value. (The image I is a *scene over* $\mathbb{Z}^n$ as defined in [41].)

When $I \equiv (E, f)$ is a binary image, we define the *foreground* of I as the subset of E $U(I) \equiv \{c \in E \mid f(c) = 1\}$. We similarly define its complement in E, the *background* of I, as $N(I) \equiv \{c \in E \mid f(c) = 0\}$. The elements of $U(I)$ are called *1-voxels* (of I) and the elements of $N(I)$ are called *0-voxels* (of I).

2.1.2 Digital m-cubes, open and closed m-cubes

The following subsets of $\mathbb{Z}^n$ or $\mathbb{R}^n$ will help us to localize the construction of continuous analogs. For any two voxels c and d, we set $\|c - d\|_1 = \sum_{i=1}^{n} |c^{(i)} - d^{(i)}|$ and $\|c - d\|_\infty = \max_{i=1,\ldots,n} |c^{(i)} - d^{(i)}|$. For $0 \leq m \leq n$, a *digital m-cube* A is a subset of $\mathbb{Z}^n$ such that two of its elements c and d satisfy both $\|c - d\|_\infty = 1$ and $\|c - d\|_1 = m$ and, for any $u \in A$, the statement $\forall 1 \leq i \leq n, c^{(i)} \leq u^{(i)} \leq d^{(i)}$ holds. A digital m-cube contains 2^m elements. In the following, digital m-cubes will conveniently be denoted by C^m (and when several are needed, by C_1^m, C_2^m, etc). The closed convex hull (in $\mathbb{R}^n$) of the voxels of a digital m-cube is called a *closed m-cube*. This convex set is clearly m-dimensional. The interior of a *closed m-cube* is called an *open m-cube* or more simply a *m-cube* (it is equal to the open convex hull of the voxels of the same digital m-cube). There is a one-to-one correspondence between digital m-cubes and (closed or open) m-cubes. Therefore, for a given digital m-cube C^m, its corresponding m-cube (respectively, closed m-cube) will be denoted by $\mathcal{C}^m$ (respectively, $\overline{\mathcal{C}}^m$). The reciprocal notations also hold. The set of all open m-cubes of $\mathbb{R}^n$, for $0 \leq m \leq n$, partitions the space $\mathbb{R}^n$ into points, edges, squares, cubes, hypercubes, etc.

If we follow the analogy with a classical iso-surface extraction technique [30], the digital 3-cubes are exactly the "cubes" of the "marching cube" algorithm.

2.1.3 Voxel adjacency, digital connectedness

Let ω_n be the binary relation on $\mathbb{Z}^n$ such that the statement $\omega_n(u, v)$ is true when $\|u - v\|_1 = 1$. Let α_n be the binary relation on $\mathbb{Z}^n$ such that the statement $\alpha_n(u, v)$ is true when $\|u - v\|_\infty = 1$. Following Herman [16] and Udupa [41], a binary relation ρ on $\mathbb{Z}^n$ is said to be an *adjacency between voxels* iff all of the following conditions are satisfied: (i) ρ is irreflexive and symmetric;

(ii) $\omega_n \subset \rho$; (iii) $\rho \subset \alpha_n$; (iv) for every three distinct voxels c, d, and e, if $\rho(c,d)$ and, for each $1 \leq j \leq n$, e_j lies between c_j and d_j then $\rho(c,e)$; (v) ρ is translation invariant, i.e., $\rho(c,d)$ implies $\rho(c+\mathbf{x}, d+\mathbf{x})$ for any voxels c, d and any integer translation vector $\mathbf{x}$. When ρ is an adjacency relation on $\mathbb{Z}^n$ and two voxels c and d are such that $\rho(c,d)$, we say that c is *ρ-adjacent* to d. Any voxel u is ρ-adjacent to a finite number of voxels.

We note that the relation ω_3 is the classical *6-adjacency* and that the relation α_3 is the classical *26-adjacency* [22]. We will use two other adjacency relations in this paper. The η_n-adjacency is defined as the binary relation on $\mathbb{Z}^n$ such that $\eta_n(u,v)$ if $\eta_n \subset \alpha_n$ and $\|u-v\|_1 \leq 2$. The μ_n-adjacency is defined as the binary relation on $\mathbb{Z}^n$ such that $\mu_n(u,v)$ if $\mu_n \subset \alpha_n$ and $\|u-v\|_1 \leq n-1$. In $\mathbb{Z}^3$, η_3 and μ_3 coincide with the classical *18-adjacency*.

Let ρ be a voxel adjacency on $\mathbb{Z}^n$. For any c and d in $A \subset \mathbb{Z}^n$, a sequence $u_0, \ldots, u_j$ of elements of A is said to be a ρ-path in A connecting c to d if $u_0 = c$, $u_j = d$, and, for $1 \leq i < j$, $\rho(u_i, u_{i+1})$. In this case, we say that c is *ρ-connected in A to d*. We note that the ρ-connectedness in A is an equivalence relation and it partitions A into *ρ-components*. A is said to be *ρ-connected* when it has exactly one component. When no confusion may arise, we will use the terms *ρ-connected* instead of *ρ-connected in A*.

2.1.4 Surfel, digital surface, boundary, $\kappa\lambda$-boundary

For any voxel c and d with $\omega_n(c,d)$, we call the ordered pair (c,d) a *surfel* (for "surface element" [16, 41]). Any nonempty set of surfels is called a *digital surface*. The *boundary* $\partial(A,B)$ between two disjoint subsets A and B of $\mathbb{Z}^n$ is defined as the set $\partial(A,B) = \{(c,d) \mid \omega_n(c,d)$ and $c \in A$ and $d \in B\}$. When not empty, it is a digital surface.

Let I be a binary image. A surfel (c,d) is called a *boundary surfel* of I if $c \in U(I)$ and $d \in N(I)$. The set of all boundary surfels of I is denoted by $\mathbb{B}(I)$. Let κ and λ be two adjacencies between voxels and let O be any κ-component of $U(I)$ and Q any λ-component of $N(I)$. The set $\partial(O,Q)$ is called a *$\kappa\lambda$-boundary of I*, provided it is not empty. It is easy to see that any boundary surfel of $\mathbb{B}(I)$ is contained in a unique $\kappa\lambda$-boundary of I.

Note that digital surfaces may also be defined as sets of voxels [21, 23, 31, 33] or as a set of squares and triangles in $\mathbb{R}^3$ [11]. In the following, digital surfaces are always sets of surfels.

2.1.5 Jordan pairs for n

As it was emphasized in the introduction, the extraction of objects and boundaries from n-dimensional images is a fundamental issue. A $\kappa\lambda$-boundary is a suitable definition for a boundary in a digital space. In the 3D space, it can be visualized as a set of closed squares parallel to axis planes. Ideally, these squares should separate 1-voxels from 0-voxels. Unfortunately, this is not always the case for arbitrary κ and λ adjacencies. This is why we need to recall other definitions and properties linked to $\kappa\lambda$-boundaries.

For any digital surface Σ, its *immediate interior* $II(\Sigma)$ is defined as the set $\{c \in \mathbb{Z}^n \mid \exists d, (c,d) \in \Sigma\}$, and its *immediate exterior* $IE(\Sigma)$ is defined as the set $\{d \in \mathbb{Z}^n \mid \exists c, (c,d) \in \Sigma\}$. A digital surface Σ is said to be *near-Jordan* if every ω_n-path from an element of $II(\Sigma)$ to an element of $IE(\Sigma)$ *exits through* Σ (i.e., there exist two consecutive voxels u_i and u_{i+1} of the ω_n-path such that $(u_i, u_{i+1}) \in \Sigma$). If every $\kappa\lambda$-boundary of every binary image in $\mathbb{Z}^n$ is near Jordan, then (κ, λ) is called a *Jordan pair for* n. It has been demonstrated in [16] that (κ, λ) is a Jordan pair for n iff (λ, κ) is a Jordan pair for n. We will thus use the unordered notation $\{\kappa, \lambda\}$ for Jordan pairs.

If $\{\kappa, \lambda\}$ is a Jordan pair for n, the $\kappa\lambda$-boundaries of any image I have the following interesting property: they separate κ-components of 1-voxels from λ-components of 0-voxels in the digital space $(\mathbb{Z}^n, \omega_n)$. They form also a partition of $\mathbb{Z}^n$ into two connected classes, one of them being finite: their *interior* elements and their *exterior* elements. These properties are very similar to the properties of connected closed $(n-1)$-dimensional manifolds in the space $\mathbb{R}^n$, which separate the space into two connected sets, one of them being finite, such that the boundary of these sets is exactly the $(n-1)$-manifold. The $\kappa\lambda$-boundaries thus define objects by their boundary, which is a convenient representation especially for $n = 3$.

Consequently, finding the Jordan pairs for any n has both theoretical and practical consequences. We show in the remainder of the paper that we can extract new Jordan pairs by building a continuous analog to $\kappa\lambda$-boundaries (see Section 4.1). Note that the definition of $\kappa\lambda$-boundary does not contain the notion of "adjacency" and "connectedness" between its elements. This notion is also important for the extraction of $\kappa\lambda$-boundary by *tracking* their elements along their adjacencies. We will tackle this issue in Section 4.3 and, for the 3D case, in Section 5.2.

2.2 Complexes

The analog of digital boundaries is built using basic elements in the Euclidean space that fit together. The *complex* is a classical tool of combinatorial topology that answers to these requirements. We present here two specific classes of complexes which are sufficient to our purpose: the Euclidean complex and the polyhedral complex. Their constitutive elements, the simplex and the convex polyhedral domain, respectively, are defined in Appendix B. Additional definitions and properties of complexes are presented in Appendix D.

A *Euclidean complex* K is a finite set of *mutually disjoint* Euclidean simplexes situated in some $\mathbb{R}^n$ such that every face of every simplex of K is also an element of K. The set K may be partially ordered as follows: a simplex $\sigma \in K$ precedes a simplex $\sigma' \in K$ (denoted by $\sigma \prec \sigma'$) if σ is a proper face of σ'. σ is *incident* to σ' if either $\sigma \prec \sigma'$ or $\sigma' \prec \sigma$. This definition is the restriction to finite complexes of the definition given in [28]. It corresponds to the definition of *triangulation* given in [2]. The *dimension* of K is the maximal dimension of its simplices.

The definition of a *polyhedral complex* is obtained by replacing the word "simplex" in the definition of Euclidean complex by "convex polyhedral domain," leaving everything else unchanged. Any p-dimensional element of a polyhedral complex K will be called a *p-cell* of K. Any Euclidean complex is a polyhedral complex. The union of the elements of K (as point sets of a given $\mathbb{R}^n$) is called the *body of the complex* K and is denoted by $\|K\|$.

Every subset K' of a complex K (either Euclidean or polyhedral) is called a *subcomplex* of K iff $\pi, \pi' \in K'$ and $\pi \prec \pi'$ in K implies $\pi \prec \pi'$ in K'. Informally, the incidence relations between elements of the subcomplex K' are the incidence relations between these elements in the complex K.

Note that any set which is the body of some Euclidean complex is called a *polyhedron*. A polyhedron may as well be defined as the body of some polyhedral complex. This definition corresponds to the intuitive notion of polyhedron. Since we will build the continuous analog locally, piece by piece, the following subcomplex will be useful:

Lemma 1. Let $\mathcal{D}$ be any *closed set* of $\mathbb{R}^n$. If L is the subcomplex of a Euclidean complex K (respectively, polyhedral complex K) whose elements are the elements of K that are a subset of $\mathcal{D}$, then L is either empty or is a Euclidean complex (respectively, polyhedral complex). This subcomplex (empty or not) will be conveniently denoted by $K \Cap \mathcal{D}$.

Proof. All elements of this subcomplex are clearly disjoint. Assuming L is not empty and $\sigma \in L$, let σ' be a face of σ in K. We have $\sigma' \subset \overline{\sigma} \subset \overline{\mathcal{D}} = \mathcal{D}$ and σ' is also in L. □

2.3 Continuous analogs of voxels

Latecki [27] defines the continuous analog of a voxel $p \in \mathbb{Z}^3$ as the closed unit cube centered at this point with faces parallel to the coordinates planes. By imposing some properties on the binary images, several interesting results can be derived from this definition (e.g., a Jordan property, all connectednesses are equivalent). Since we wish to deal with arbitrary images, we take an opposite approach: instead of imposing some properties on binary images, we constrain the set of possible adjacency relations between voxels.

Therefore, we propose a different way to map a set of voxels into the Euclidean space. This mapping is dependent on the digital connectedness chosen for this set of voxels. By this way, connected components in the digital space are also connected in the Euclidean space. Refer to Appendix B for classical definitions related to arbitrary dimensional convex sets.

Definition 2 (ρ-decomposition of $\mathbb{Z}^n$). Let ρ be an adjacency relation in $\mathbb{Z}^n$. We define the *ρ-decomposition* $\mathcal{G}_\rho(\mathbb{Z}^n)$ of $\mathbb{Z}^n$, as the aggregate of subsets of $\mathbb{R}^n$ the elements of which are defined by:

(i) all the voxels of $\mathbb{Z}^n$ as points of $\mathbb{R}^n$ (called the 0-*cells* of the decomposition);

(ii) All the open segments of $\mathbb{R}^n$ between 0-cells when the corresponding voxels are ρ-adjacent (called the *1-cells* of the decomposition);

(iii) For $2 \leq j \leq n$, all the j-dimensional convex polyhedral domains whose boundary is composed of disjoint i-cells, $0 \leq i < j$, and that are *minimal*: $\forall \phi, \psi \in \mathcal{G}_\rho(\mathbb{Z}^n) \quad \phi \subset \psi \Rightarrow \phi = \psi$. These elements are called the j-*cells* of the decomposition.

Note that $\mathcal{G}_{\omega_n}(\mathbb{Z}^n)$ is the standard cubical partition of the space $\mathbb{R}^n$ into vertices, edges, squares, cubes, hypercubes, etc. Hence, any m-cube is an element of $\mathcal{G}_{\omega_n}(\mathbb{Z}^n)$. Any i-cell from a ρ-decomposition is built on 0-cells (the extremal points of its closure are 0-cells). By analogy with polyhedra, the 0-cells bordering an i-cell ϕ (i.e., the set $\mathrm{Extr}(\overline{\phi})$) are called the *vertices*

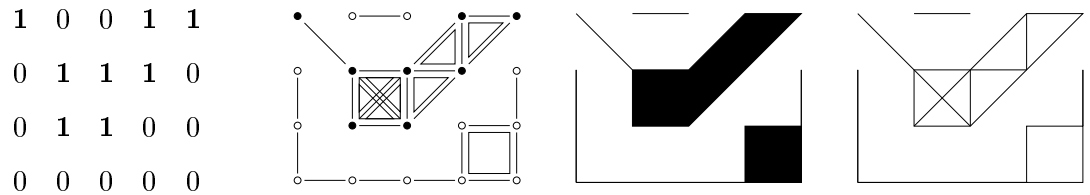

Figure 1: (a) Binary image I as a set of 0 and 1 in a digital space; (b) 8-decomposition of the foreground of I and 4-decomposition of the background of I; (c) corresponding 8-volume and 4-volume of the same sets (as subset of $\mathbb{R}^3$); (d) corresponding 8-1-skeleton and 4-1-skeleton of the same sets (as subset of $\mathbb{R}^3$).

of ϕ. By definition, these vertices are voxels of $\mathbb{Z}^n$. The aggregate $\mathcal{G}_\rho(\mathbb{Z}^n)$ is generally not a polyhedral complex.

We can define the *ρ-decomposition* $\mathcal{G}_\rho(A)$ of any subset $A \subset \mathbb{Z}^n$ as the set $\mathcal{G}_\rho(A) = \{\phi \in \mathcal{G}_\rho(\mathbb{Z}^n) \mid \mathrm{Extr}(\overline{\phi}) \subset A\}$. The 0-cells of $\mathcal{G}_\rho(A)$ are the elements of A.

Now we define a continuous analog of any set of voxels considered with an adjacency relation into the space $\mathbb{R}^n$. Informally speaking, any set of voxels fills a part of the space $\mathbb{R}^n$ that depends on the adjacency chosen for this set. In $\mathbb{R}^3$, this definition is closely related to the definition of *digital polyhedra* [21]. A digital polyhedron is created by collecting all *discrete simplexes* defined by each possible digital 3-cube of the image. However, the authors of [21] restrict their study to objects whose boundary is a cellular complex. Besides, the construction of digital polyhedra is based on the use of a table of simplexes, which is given as is: proofs cannot be derived from that kind of formulation.

Definition 3 (ρ-volume and ρ-m-skeleton). The *ρ-volume* of a set of voxels A is the subset of $\mathbb{R}^n$ that is the union (in $\mathbb{R}^n$) of all the elements of $\mathcal{G}_\rho(A)$. We call *ρ-m-skeleton* of A, for $0 \leq m \leq n$, the subset of $\mathbb{R}^n$ that is the union (in $\mathbb{R}^n$) of all the i-cells of $\mathcal{G}_\rho(A)$, for $0 \leq i \leq m$. The ρ-m-skeletons of A are thus subsets of the ρ-volume of A.

Figure 1 illustrates the notion of ρ-decomposition and of ρ-volume of sets of voxels. The ρ-volume of A is a convenient continuous analog of voxels because of the following proposition, which states that the digital connectedness property of a set of voxels is equivalent to the con-

nectedness property of its continuous analog, when $n \leq 3$ (see complete proof in Appendix C):

Proposition 4. The following three statements are equivalent, if A is a finite set of voxels and ρ an adjacency relation:

(i) (arbitrary n) the set A is ρ-connected,

(ii) (arbitrary n) the ρ-1-skeleton of A is connected,

(iii) ($n \leq 3$) the ρ-volume of A is connected.

and (i) $\Rightarrow$ (iii) and (ii) $\Rightarrow$ (iii) for arbitrary n.

The whole Proposition 4 is true also for the adjacency relations α_n and ω_n for arbitrary n. Although we have not found any counterexample, we do not know yet whether or not Proposition 4 is true for any ρ and n. In the 3D case, this proposition entails that if a set of voxels A has k ρ-connected components, then its continuous analog, the ρ-volume of A, has also k connected components. This equivalence will be especially useful finding new Jordan pairs for n, where only the equivalence (i) $\Leftrightarrow$ (ii) will be used in the proof (Theorem 29).

2.4 Specific adjacencies

In order to build a surface in $\mathbb{R}^3$ (or a set in $\mathbb{R}^n$) separating the 1-voxels from the 0-voxels of a binary image I, we must add two additional constraints on the adjacency relations with which these sets are considered: the first is linked to the embedding of the voxels in $\mathbb{R}^n$ (i.e., if these two embeddings intersect, then there is no possible way to build a surface separating them), the other is linked to the way this "surface" is built (i.e., the surface is built piece by piece; these pieces must fit together).

Definition 5 (Proper adjacency pair). A pair $\{\kappa, \lambda\}$ of adjacency relations between voxels is said to be *proper* if for any two disjoint sets A, B of voxels, all the elements of $\mathcal{G}_\kappa(A)$ are disjoint from all the elements of $\mathcal{G}_\lambda(B)$.

It is easy to see that any pair $\{\omega_n, \rho\}$ is proper, and, for any $\rho \neq \omega_n$, the pair $\{\rho, \alpha_n\}$ is not proper. Further, if $\{\kappa, \lambda\}$ is proper, then any $\{\kappa', \lambda'\}$, $\kappa' \subset \kappa$ and $\lambda' \subset \lambda$, is proper.

Clearly, the fact that a pair of adjacency relations is proper is a necessary condition to build a continuous analog to a $\kappa\lambda$-boundary that separates continuous analogs of the foreground from continuous analogs of the background. We have the following simple lemma:

Lemma 6. For $n \geq 3$, if $\eta_n \subset \kappa$ and $\{\kappa, \lambda\}$ is proper, then $\lambda = \omega_n$.

Proof. It is sufficient to consider the case of two diagonally opposite voxels in a digital 2-cube. Point (iv) of the voxel adjacency definition concludes the argument. □

We introduce the following definition, which will be useful in the case $n = 2$: a pair $\{\kappa, \lambda\}$ of adjacency relations between voxels is said to be *connecting* when, for any binary image I and any digital n-cube C^n of I, either the set of 1-voxels in C^n is κ-connected or the set of 0-voxels in C^n is λ-connected.

The continuous analog of a digital boundary is constructed n-cube by n-cube. Each piece constructed in a digital n-cube must fit with the pieces built in the adjacent digital n-cubes. Consequently, we introduce the following definition, whose purpose will clearly appear in the remainder of the paper (see Section 3.2.1):

Definition 7 (quasi-complete adjacency). Any adjacency relation ρ between voxels is said to be *quasi-complete* if $\mu_n \subset \rho$.

Note that α_n is quasi-complete, ω_n is not quasi-complete for any $n > 2$, η_n is not quasi-complete for any $n > 3$. An immediate corollary to Lemma 6 is:

Lemma 8. For $n \geq 3$, if κ is quasi-complete and $\{\kappa, \lambda\}$ is proper, then $\lambda = \omega_n$ and $\{\kappa, \lambda\}$ is connecting.

3 Continuous analogs of digital boundaries

Starting from any binary image I (possibly obtained by thresholding a gray-level image), we would like to build a continuous analog to any $\kappa\lambda$-boundary of I, if (κ, λ) is the connectedness pair chosen for the foreground and for the background of I.

Following the analogy with iso-surface extraction techniques, we propose a local approach to this construction. In [30], the authors build an iso-surface locally on each group of eight adjacent

(26-adjacent) voxels forming a cube. Within each "cube," a set of triangles is extracted. The algorithm "marches" on all "cubes" of the image to extract the whole triangulated surface. Each "cube" shares "faces" of four voxels with adjacent "cubes." With this property, the triangles built within a "cube" theoretically fit with the triangles built within an adjacent "cube."

In fact, this was not exactly the case in the original paper, and the whole set of triangles did not form a closed surface, as classically defined (a 2-manifold without boundary): some holes are present in the set. Different approaches have been proposed to correct the so-called "topological ambiguity" problem of the marching cubes [14, 34, 35, 36, 38]. None of the proposed methods are explicitly based on the introduction of digital connectedness.

The continuous analog of a $\kappa\lambda$-boundary in a binary image will provide a formal way to build *locally* a surface (or hypersurface in arbitrary dimension) separating two sets. As it is shown in Section 5, the continuous analog will nicely correspond to the usual definition of iso-surface in the 3D case.

We begin by mapping the elements of a digital boundary (i.e., the boundary surfels) into the Euclidean space and then we present the construction of the continuous analog as a *polyhedral complex* whose vertices are the mapped boundary surfels.

3.1 Mapping boundary surfels into $\mathbb{R}^n$

The first step in constructing a continuous analog to digital $\kappa\lambda$-boundaries is to map their elements into $\mathbb{R}^n$. Let I be any binary image in $\mathbb{Z}^n$ and $\mathbb{B}(I)$ its set of all boundary surfels. Any mapping h from the space $\mathbb{B}(I)$ to the space $\mathbb{R}^n$ is called a *boundary mapping of I into* $\mathbb{R}^n$ if, for $t = (c, d) \in \mathbb{B}(I)$, $h(t)$ lies in the open segment of $\mathbb{R}^n$ whose endpoints are c and d.

This definition of boundary mapping is particularly useful in the context of the computation of an iso-surface within a gray-level image. Indeed, let $J = (E, f)$ be a gray-level image in $\mathbb{Z}^n$ and let s be an iso-value. The thresholded image $J_s = (E, f_s)$ is a binary image ($f(v) \leq s \Rightarrow f_s(v) = 0$ and $f(v) > s \Rightarrow f_s(v) = 1$). It contains a set of boundary surfels $\mathbb{B}(J_s)$. Let h_s be a mapping from $\mathbb{B}(J_s)$ to $\mathbb{R}^n$ such that:

$$h_s : (u, v) \in \mathbb{B}(J_s) \longmapsto h_s(u, v) = \left(1 - \frac{s - f(u)}{f(v) - f(u)}\right) u + \left(\frac{s - f(u)}{f(v) - f(u)}\right) v.$$

It is easy to verify that h_s is a boundary mapping of J_s into $\mathbb{R}^n$ *when* f *does not take the value* s *on any of the voxels of* J. Notice that, if $s = f(c)$ for some voxel c in E, then the mapping h_s may not be one-to-one any more. Since we cannot build a polyhedral complex on vertices that are not all pairwise disjoint, we will always assume in the following that either $s \neq f(c)$ for any voxel c in E or h_s is built in such a way that it is a boundary mapping of J_s into $\mathbb{R}^n$.

The boundary mapping h_s gives the linear approximation of the intersection of the iso-potential set defined by s with the segments between adjacent voxels. It is similar to the linear approximation of the surface–edge intersection of the marching cube [30]. Note that if the negative image of J_s is J_s^-, then we can define a *negative boundary mapping* h_s^- from $\mathbb{B}(J_s^-)$ to $\mathbb{R}^n$ such that $h_s^-(v,u) = h_s(u,v)$ since $(v,u) \in \mathbb{B}(J_s^-) \Leftrightarrow (u,v) \in \mathbb{B}(J_s)$. The algebraic expression of h_s^- is identical to the expression of h_s (only the domain changes).

Most of the results we are presenting in this paper are *independent* of the chosen boundary mapping for a given image. Only the geometry of the continuous analog is dependent on it. The boundary mapping highlights the fact that the continuous analog of a digital boundary can be interpreted as a triangulated approximation of some iso-potential set. In particular, the continuous analog coincides with a triangulated iso-surface for the case $n = 3$ (see Section 5). When a binary image I does not come from the thresholding of a gray-level image, any boundary mapping can be chosen for I; for some figures, the *trivial boundary mapping* $g : (u,v) \in \mathbb{B}(I) \mapsto (u+v)/2$ will be conveniently used.

For any image I and any boundary mapping h of I, the elements of $h(\mathbb{B}(I))$ are called *boundary vertices induced by* h (or simply *boundary vertices* when no confusion may arise). The set of all the boundary vertices of I induced by h is denoted by $\mathcal{A}_h(I)$. The mapping h is a one-to-one mapping from $\mathbb{B}(I)$ to $\mathcal{A}_h(I)$. If O is a set of 1-voxels in I, we will also use the notation $\mathcal{A}_h(O)$ to designate the boundary vertices $h(u,v)$ with $u \in O$. If C is any set of voxels, the notation $\mathcal{A}_h(O,C)$ indicates the subset of $\mathcal{A}_h(O)$ whose elements $h(u,v)$ follow $u \in O$ and $v \in C$.

3.2 Continuous analog definition

In this section, we use the following notations: I is a binary image and h a boundary mapping of I, O is a κ-connected component of 1-voxels in I, Q is a λ-connected component of 0-voxels

in I, Σ is the $\kappa\lambda$-boundary of O and Q (supposed to be nonempty). The adjacency pair $\{\kappa, \lambda\}$ is supposed to be proper and connecting. We define the continuous analog of a $\kappa\lambda$-boundary in four steps:

1. First, we define the *local volume* $\mathcal{V}_h(O, C^n)$ within each digital n-cube C^n of the image that meets O. The local volume can be seen as one or two bricks whose vertices are boundary vertices and 1-voxels of O.

2. If the adjacency κ is quasi-complete, then all these bricks fit well together. In this case, the set of all the bricks created in every digital n-cube meeting O forms a n-dimensional polyhedral complex $K_h(O)$, called the *solid extension of* O. The solid extension of O contains the ρ-volume of O and excludes the λ-volume of any set of voxels disjoint from O, e.g., Q.

3. The *boundary* $\mathfrak{B}K_h(O)$ of the solid extension of O is itself a $(n-1)$-polyhedral complex which is composed of several connected components. The set of vertices of $\mathfrak{B}K_h(O)$ is exactly the set of boundary vertices $\mathcal{A}_h(O)$.

4. The *continuous analog* $\mathcal{S}_h(O, Q)$ of the $\kappa\lambda$-boundary $\partial(O, Q)$ is defined as the body of the *unique* connected component of $\mathfrak{B}K_h(O)$ that borders Q. It is a (strongly) connected polyhedron that separates the space $\mathbb{R}^n$ in two connected domains. The set of vertices of this polyhedron is exactly the set of boundary vertices $\mathcal{A}_h(O, Q)$.

The following four subsections detail these four steps. Figure 2 depicts the local construction of the continuous analog with a 3D example. The necessity of $\{\kappa, \lambda\}$ to be proper has already been stressed. The necessity of κ to be quasi-complete will be exhibited in the following subsection. The connecting property of $\{\kappa, \lambda\}$ is useful only in the case $n = 2$ (see Lemma 8) and is needed in the demonstration of Lemma 24 (Section 3.2.4).

3.2.1 Local volume, local complex

In this section, C^n is a digital n-cube which contains at least one voxel of O, and C^m is a digital m-cube that is included in C^n (obviously $m \leq n$).

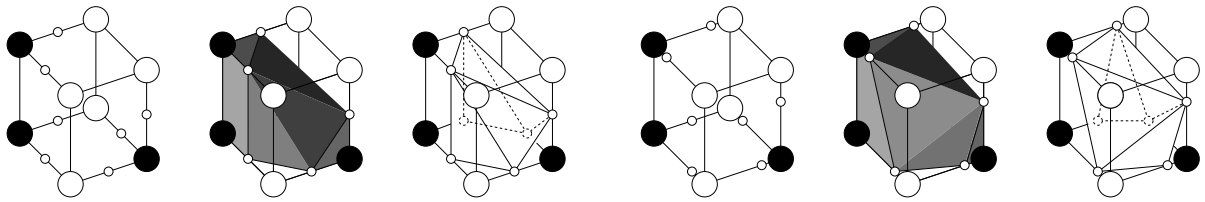

(a) (b) (c) (d) (e) (f)

Figure 2: This figure illustrates how to build locally the $\kappa\lambda$-continuous analog of $\mathbb{B}(I)$: (a) the digital 3-cube C^3 with the value in I of its voxels (black: 1, white: 0) together with the boundary vertices (small circles) $\mathcal{A}_g(U(I) \cap C^3, N(I) \cap C^3)$, where g is the trivial boundary mapping; (b) the C^3-local volume of $U(I)$ induced by h; (c) deletion of every cell with a 1-voxel vertex; (d) same as (a) but with an arbitrary boundary mapping h (surfels may not be mapped at midpoints); (e) same as (b) but with h; (f) same as (c) but with h. The boundary mapping does not influence the edges on the 2-faces of the digital n-cube.

Definition 9 (C^n-local volume). Let $P_1, \ldots, P_l$ be the κ-connected components of $O \cap C^n$. The *C^n-local volume of O induced by h*, denoted by $\mathcal{V}_h(O, C^n)$, is the subset of $\mathbb{R}^n$ defined as

$$\bigcup_{i=1..l} \mathrm{Conv}(P_i \cup \mathcal{A}_h(P_i, C^n)).$$

In other words, the local volume is composed of several n-dimensional closed convex sets, one for each κ-connected component of O in this digital n-cube. These convex sets are defined by the location of the voxels in $\mathbb{R}^n$ and by the location of the boundary vertices bordering these voxels in this n-cube. We similarly define the *C^m-local volume of O induced by h*, $0 \leq m \leq n$, by changing the symbol C^n with the symbol C^m in the previous definition.

It is straighforward to see that $\mathcal{V}_h(O, C^m) \subset \overline{\mathcal{C}}^m$, for any h. The boundary mapping h influences the shape of the local volume, but under certain conditions, not its topology, as the following lemma shows:

Lemma 10. If the adjacency κ is quasi-complete, the number of connected components of $\mathcal{V}_h(O, C^m)$ is equal to the number of κ-connected components of $O \cap C^m$. More precisely, this number is equal to one or two when $m = n$ and is equal to zero or one when $m < n$.

Proof. The case where $\mathcal{V}_h(O, C^m)$ is empty is trivial. The lemma obviously holds if $O \cap C^m$ is κ-connected and this statement is always true when $m < n$ since by definition $\kappa \supset \mu_n$. Assume

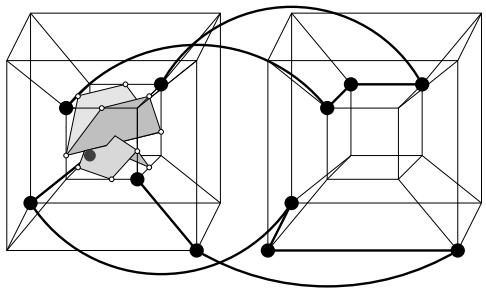

Figure 3: This figure illustrates that the local volume of two disconnected sets of voxels might be connected when the adjacency relation is not quasi-complete. This counterexample occurs in $\mathbb{R}^5$ with the ω_5-adjacency. The digital 5-cube is seen as two adjacent digital 4-cubes. The voxels adjacency is represented by thick lines.

$m = n$ and $O \cap C^m$ is not κ-connected. The definition of quasi-complete adjacency implies that $O \cap C^n$ is a set of two diagonally opposite voxels in C^n, say u and v. Now the convex set $\mathcal{U} = \mathrm{Conv}(u \cup \mathcal{A}_h(u, C^n))$ forms a corner of the closed n-cube $\overline{\mathcal{C}}^n$, for any h. The set $\overline{\mathcal{C}}^n \setminus \mathcal{U}$ is therefore convex. Now, for any h, the voxel v and any element of $\mathcal{A}_h(v, C^n)$ are in $\overline{\mathcal{C}}^n \setminus \mathcal{U}$: their closed convex hull is therefore in $\overline{\mathcal{C}}^n \setminus \mathcal{U}$ and the two convex sets forming $\mathcal{V}_h(O, C^n)$ are disjoint. □

Figure 3 shows that this property is not true in general if the adjacency is not quasi-complete. The following lemma is a direct consequence of Lemma 10 and of point (iv) of the definition of adjacency between voxels:

Lemma 11. If the adjacency κ is quasi-complete, we have $\mathcal{V}_h(O, C^m) = \mathcal{V}_h(O, C^n) \cap \overline{\mathcal{C}}^m$.

Note that the hypothesis of κ quasi-completeness is a necessary and sufficient condition for Lemma 11 to be true for any binary image I. Suppose κ is not quasi-complete. Let the domain of some image I' be the image composed of two digital n-cubes C_1^n and C_2^n sharing a digital $(n-1)$-cube C^{n-1}. We also suppose that $C_1^n \setminus C^{n-1}$ is composed of 1-voxels, $C_2^n \setminus C^{n-1}$ is composed of 0-voxels, and C^{n-1} is composed of 0-voxels except two 1-voxels which are not κ-adjacent (it is possible since $\kappa \not\supset \mu_n$). The set O' of 1-voxels of I' is clearly κ-connected and the set of 0-voxels of I' is clearly λ-connected. Now $\mathcal{V}_h(O', C_1^n) \cap \overline{\mathcal{C}}^{n-1}$ is connected whereas $\mathcal{V}_h(O', C_2^n) \cap \overline{\mathcal{C}}^{n-1}$ is not connected.

Consequently, given two different closed n-cubes that share some vertices (i.e., a closed k-cube), their local volumes are identical on their common face. Lemma 11 complemented by the following lemma shows that the "bricks" fit well together:

Lemma 12. When the adjacency κ is quasi-complete and $m < n$, the set $\mathcal{V}_h(O, C^m)$ is either empty or a closed polyhedral domain that is m-dimensional.

Proof. Because κ is quasi-complete, the set $\mathcal{V}_h(O, C^m)$ is connected and is trivially a closed polyhedral domain. We now compute its dimension. By definition, the 0-faces of $\mathcal{V}_h(O, C^m)$ are among $(O \cap C^m) \cup \mathcal{A}_h(O, C^m)$. It is easy to see that all these points are extremal points (i.e., 0-faces) of $\mathcal{V}_h(O, C^m)$. When nonempty, at least one voxel of $O \cap C^m$ or one boundary vertex in $\mathcal{A}_h(O, C^m)$ is a 0-face of $\mathcal{V}_h(O, C^m)$. If it is a boundary vertex, it is clear that $O \cap C^m$ is also not empty. Therefore, at least one voxel of O (say u) is a 0-face of $\mathcal{V}_h(O, C^m)$. If we look at the m ω_n-neighbors of u that are also in C^m, then two cases arise: either this neighbor is in O and hence is included in $\mathcal{V}_h(O, C^m)$, or this neighbor is not in O and a boundary vertex is located in-between: this boundary vertex is also included in $\mathcal{V}_h(O, C^m)$. We have found m points in $\overline{\mathcal{C}}^m$, which are linearly independent and included in a convex set. This convex set is thus at least m-dimensional. Because the set $\mathcal{V}_h(O, C^m) \subset \overline{\mathcal{C}}^m$, it must be exactly m-dimensional. □

Supposing the adjacency κ is quasi-complete, Lemma 10 implies that the C^n-local volume is composed of one or two disjoint convex sets, which are the closure of convex polyhedral domains. Therefore, we can define:

Definition 13 (C^n-local complex). When the adjacency κ is quasi-complete, the set $\mathcal{V}_h(O, C^n)$ is the disjoint union of one or two n-dimensional closed polyhedral domains. The n-dimensional polyhedral complex, such that its n-cells are the interior of these closed polyhedral domains and all its other cells are the faces of these n-cells, is called the *C^n-local complex of O induced by h*, and is denoted by $V_h(O, C^n)$. Thus, the body of $V_h(O, C^n)$, i.e., $\|V_h(O, C^n)\|$, is by definition equal to $\mathcal{V}_h(O, C^n)$.

Furthermore, when $m < n$ and $O \cap C^m \neq \emptyset$, the set $\mathcal{V}_h(O, C^m)$ is one m-dimensional closed polyhedral domain (Lemma 12). The m-dimensional polyhedral complex, such that its m-cell is the interior of this closed polyhedral domain and all its other cells are the faces of this m-cell, is called the *C^m-local complex of O induced by h*, and it is denoted by $V_h(O, C^m)$. (By

definition, $\|V_h(O, C^m)\| = \mathcal{V}_h(O, C^m)$.) If $O \cap C^m = \emptyset$, it is conveniently defined as the empty set.

In fact, the complex $V_h(O, C^m)$ is a particular subcomplex of $V_h(O, C^n)$:

Lemma 14. When κ is quasi-complete, the equality $V_h(O, C^m) = V_h(O, C^n) \Cap \overline{\mathcal{C}}^m$ holds.

Proof. The equality is trivial if $m = n$ or if $O \cap C^m = \emptyset$. Suppose $m < n$ and $O \cap C^m \neq \emptyset$. The set $\mathcal{V}_h(O, C^n)$ is made of one or two components (each is a closed polyhedral domain), and only one, say π^n, touches $\overline{\mathcal{C}}^m$. Now the m-plane carrying $\overline{\mathcal{C}}^m$ can be seen as the intersection of $n - m$ supporting planes of π^n. Lemma 11 and Lemma 12 imply that the interior of $\mathcal{V}_h(O, C^m)$ is an m-dimensional face of π^n. Any element of $V_h(O, C^m)$ is thus in $V_h(O, C^n) \Cap \overline{\mathcal{C}}^m$. As well, any element of $V_h(O, C^n) \Cap \overline{\mathcal{C}}^m$ is a face of the m-cell of $V_h(O, C^m)$. □

The following lemma expresses the idea that local complex cells intersecting an open face of a n-cube are completely included in this open face:

Lemma 15. Assume κ is quasi-complete. Let $\pi \in V_h(O, C^n)$. If $\pi \cap \mathcal{C}^m \neq \emptyset$, then $\pi \subset \mathcal{C}^m$ and $\pi \in V_h(O, C^m)$.

Proof. The lemma is obvious if $m = n$. Suppose $m < n$. Let R^m be the carrying plane of $\overline{\mathcal{C}}^m$. The m-plane R^m is the intersection of $n - m$ supporting planes $R_1^{n-1}, \ldots, R_{n-m}^{n-1}$ of the convex polyhedral domain $\mathcal{C}^n$. We can choose these planes so that the set $\mathcal{C}^n$ be included in all the open positive (say) half-spaces $H_1, \ldots, H_{n-m}$ that are respectively bounded by $R_1^{n-1}, \ldots, R_{n-m}^{n-1}$. Let ϕ be the open convex hull of some points which are either in $\overline{\mathcal{C}}^m$ or in $\overline{\mathcal{C}}^n \setminus \overline{\mathcal{C}}^m$. If any one of them is in the latter set, then it does not belong to at least one R_i^{n-1}, hence is included in the open positive half-space H_i. By definition of the open convex hull as a linear combination with strictly positive coefficients, it is clear that ϕ is totally included in H_i, hence has an empty intersection with R_i^{n-1}, furthermore with $\overline{\mathcal{C}}^m$.

Now the set π is the open convex hull of the extremal points of $\overline{\pi}$. If any of these extremal points are not in $\overline{\mathcal{C}}^m$, the previous discussion concludes that $\pi \cap \overline{\mathcal{C}}^m = \emptyset$, which is a contradiction with the hypothesis. All extremal points of $\overline{\pi}$ are thus in $\overline{\mathcal{C}}^m$. The Krein–Milman theorem implies that $\overline{\pi} \subset \overline{\mathcal{C}}^m$. Since π^m is open in its carrying plane, we have $\pi^m \subset \mathcal{C}^m$. Clearly, $\pi^m \in V_h(O, C^n) \Cap \overline{\mathcal{C}}^m$. Lemma 14 concludes. □

3.2.2 Solid extension

In this section, we assume that the adjacency κ is quasi-complete. We construct an n-dimensional complex, which includes both the voxels of O and the boundary vertices of O, by gathering all local complexes of O:

Definition 16 (Solid extension of O). Let $K_h(O)$ be the set obtained by collecting all elements of the C^n-local complexes of O according to the following rule: if a p-cell, $0 \leq p \leq n$, belongs to one or more local complexes, then this p-cell is present only once in $K_h(O)$ and collects all the incidence properties that it had in those local complexes. The set $K_h(O)$ is called the *solid extension of O induced by h*.

We show that this assembly of complexes constructs a polyhedral complex:

Proposition 17. The set $K_h(O)$ is an n-dimensional polyhedral complex.

Proof. The definition of $K_h(O)$ entails that the faces of any element of the complex $K_h(O)$ are also element of this complex. It remains to show that all elements of $K_h(O)$ are mutually disjoint. Let π_1 and π_2 be two elements of $K_h(O)$, $\pi_1 \neq \pi_2$. Then there exist two digital n-cubes, say C_1^n and C_2^n, such that $\pi_1 \in V_h(O, C_1^n)$ and $\pi_2 \in V_h(O, C_2^n)$. If $C_1^n = C_2^n$ then $\pi_1 \cap \pi_2 = \emptyset$ since $V_h(O, C_1^n)$ is a polyhedral complex. If $C_1^n \cap C_2^n = \emptyset$ then $\pi_1 \cap \pi_2 = \emptyset$ because $\pi_1 \subset \|V_h(O, C_1^n)\| \subset \overline{\mathcal{C}}_1^n$ and $\pi_2 \subset \|V_h(O, C_2^n)\| \subset \overline{\mathcal{C}}_2^n$ and $\overline{\mathcal{C}}_1^n \cap \overline{\mathcal{C}}_2^n = \emptyset$. If $C_1^n \cap C_2^n \neq \emptyset$ then their intersection is a digital m-cube C^m. If $\pi_1 \cap \overline{\mathcal{C}}^m = \emptyset$ or $\pi_2 \cap \overline{\mathcal{C}}^m = \emptyset$ then $\pi_1 \cap \pi_2 = \emptyset$. Otherwise, Lemma 15 induces π_1 and π_2 are both element of the same polyhedral complex $V_h(O, C^m)$. They are thus disjoint. □

We derive two fundamental properties of the solid extension:

Lemma 18. Any $(n-1)$-cell of $K_h(O)$ is either the face of two n-cells when it is included in some closed $(n-1)$-cube, or the face of one n-cell (when it is included in an n-cube).

Proof. Let π be a $(n-1)$-cell of $K_h(O)$. Let us assume that π is included in some closed $(n-1)$-cube, whose corresponding digital $(n-1)$-cube is C^{n-1} (say). This digital $(n-1)$-cube belongs to exactly two digital n-cubes. According to Lemma 15, π is the $(n-1)$-cell of the

complex $V_h(O, C^{n-1})$. Lemma 14 induces that π is a $(n-1)$-face of exactly one n-cell in one of these n-cubes and is a $(n-1)$-face of exactly one n-cell in the other n-cube. Because π is open and $(n-1)$-dimensional, it is a subset of $\mathcal{C}^{n-1}$, and therefore cannot be the face of any other n-cell. If π is not included in some closed $(n-1)$-cube, then Lemma 15 implies that π is a subset of an open n-cube. Within this n-cube, it is the face of exactly one n-cell (the convex polyhedral domain that defines it). □

Lemma 19. The n-dimensional complex $K_h(O)$ is strongly connected.

Proof. The idea is to use the κ-connectedness of the set O to build a path of digital n-cubes such that any two consecutive digital n-cubes share a digital $(n-1)$-face. Let π and π' be two n-cells of $K_h(O)$. Let u be a voxel of O bordering π and u' be a voxel of O bordering u'. Because O is κ-connected, there exists a κ-path $\Omega = o_1 o_2 \dots o_l$ in O from u to u' ($u = o_1$ and $u' = o_l$). We can build a chain Γ' of digital n-cubes, $\Gamma' = C_1^n C_2^n \dots C_{l-1}^n$, such that $\forall i, 1 \leq i \leq l-1, \{o_i, o_{i+1}\} \subset C_i^n$. We can form a new chain Γ from Γ' by setting $\Gamma = C_0^n \Gamma' C_l^n$, with $\pi \subset \overline{\mathcal{C}}_0^n$ and $\pi' \subset \overline{\mathcal{C}}_l^n$. We conveniently set $o_0 = o_1$ and $o_{l+1} = o_l$.

We show by induction on i that the following statement is true for $0 \leq i \leq l$: there is a chain of n-cells from π to a n-cell ϕ_i, with $\phi_i \subset \mathcal{C}_i^n$ and both o_i and o_{i+1} are vertices of ϕ_i, such that any two consecutive n-cells of this chain share a $(n-1)$-cell as a common face.

It is trivially true for $i = 0$. Let us assume the preceding statement is true for an $i < l$, and we show it for $i+1$. If the two n-cubes C_i^n and C_{i+1}^n are identical, we can conclude directly. Otherwise, the voxel o_{i+1} belongs to both C_i^n and C_{i+1}^n. A chain Λ of at most $n-1$ digital n-cubes containing o_{i+1} can be constructed between C_i^n and C_{i+1}^n with the property that two consecutive digital n-cubes have a digital $(n-1)$-cube in common (by pivoting around o_{i+1}, changing one coordinate at each step). Let D and E be two consecutive elements of Λ sharing a digital $(n-1)$-cube C^{n-1}. According to Lemma 14, $V_h(O, D) \cap \overline{\mathcal{C}}^{n-1} = V_h(O, E) \cap \overline{\mathcal{C}}^{n-1} = V_h(O, C^{n-1})$. Since o_{i+1} belongs to both complexes, the complex $V_h(O, C^{n-1})$ is by definition $(n-1)$-dimensional. Its $(n-1)$-cell is a face of the n-cell of $V_h(O, D)$ incident to o_{i+1} and is a face of the n-cell of $V_h(O, E)$ incident to o_{i+1}. If we denote by ϕ_{i+1} the n-cell of C_{i+1}^n incident to o_{i+1}, the chain Λ connects $\phi_i \subset \mathcal{C}_i^n$ to $\phi_{i+1} \subset \mathcal{C}_{i+1}^n$ by n-cells sharing a common $(n-1)$-cell. Because o_{i+2} is κ-adjacent to o_{i+1}, the voxel o_{i+2} is also a vertex a ϕ_{i+1}. Since ϕ_{i+1} is connected to ϕ_i, it

is connected to π by hypothesis. The statement is demonstrated . We conclude the proof by setting $i = l$ and by noticing that ϕ_l can be set equal to π'. □

Lemma 18 and Lemma 19 lead to the following theorem (orientability is easily demonstrated):

Theorem 20. Any simplicial subdivision of the solid extension of O induced by h is a (orientable) n-pseudomanifold with boundary.

3.2.3 Boundary of the solid extension

The *boundary* of $K_h(O)$, denoted $\mathfrak{B}K_h(O)$, is the subcomplex of $K_h(O)$ whose cells are (i) all $(n-1)$-cells of $K_h(O)$ that are the face of exactly one n-cell of $K_h(O)$ and (ii) all faces of these $(n-1)$-cells. It is clearly a polyhedral complex. The following proposition states that the vertices of the complex $\mathfrak{B}K_h(O)$ are exactly the elements of $\mathcal{A}_h(O)$:

Proposition 21. The complex $\mathfrak{B}K_h(O)$ is a $(n-1)$-dimensional polyhedral complex whose vertices are the boundary vertices of O in I (i.e., the 0-cells of $\mathfrak{B}K_h(O)$ are the points of $\mathcal{A}_h(O)$).

Proof. Let π be a $(n-1)$-cell of $\mathfrak{B}K_h(O)$ and let R^{n-1} be its carrying $(n-1)$-plane. The cell π is a face of a n-cell π' of $V_h(O, C^n)$. Assume, to the contrary, that there is one vertex of π, say u, that is a voxel element of O. The set of n voxels in C^n ω_n-adjacent to u forms with u an orthonormal basis of $\mathbb{R}^n$. This basis defines an orthant in $\mathbb{R}^n$, which contains $\overline{\mathcal{C}}^n$. Lemma 18 implies that π is a subset of the n-cube $\mathcal{C}^n$. Consequently, its carrying plane R^{n-1} divides the cube $\overline{\mathcal{C}}^n$ in two parts; it also divides this orthant in two. Two endpoints of this basis, say v and w, must be in two different parts of $\mathbb{R}^n \setminus R^{n-1}$. By definition, $\omega_n(u, v)$ and $\omega_n(u, w)$. If $v \notin O$, then there exists a boundary vertex a in $\mathcal{A}_h(O)$ that belongs to the open segment bounded by u and v. Since $u \in R^{n-1}$, a must be in the same part of $\mathbb{R}^n \setminus R^{n-1}$ as v. We also have $a \in \mathcal{V}_h(O, C^n)$ and a is incident to π'. We set $v' = a$. If $v \in O$ then $v \in \mathcal{V}_h(O, C^n)$ and v is incident to π'; in this case, we set $v' = v$. With a similar reasonning for w, we obtain a point w' that is included in $\mathcal{V}_h(O, C^n)$ and that is incident to π'. We have found two points of the closed polyhedral domain $\overline{\pi'}$ that are on either side of the plane R^{n-1}. Therefore this plane is

not a supporting plane of π', which is a contradiction to the hypothesis. All the vertices of π are thus boundary vertices. It is easy to see that all boundary vertices of O are indeed 0-cells of $K_h(O)$. □

We can verify that the continuous analog of a connected component of 1-voxel is entirely included in its solid extension, whatever is the chosen boundary mapping. Furthermore, these voxels are the only voxels of $\mathbb{Z}^n$ that are included in this solid extension.

Theorem 22. The κ-volume of O is included in $\|K_h(O)\|$ and has an empty intersection with $\|\mathfrak{B}K_h(O)\|$. The λ-volume of any set of voxels in the complement of O has an empty intersection with $\|K_h(O)\|$.

Proof. Let ϕ be any i-cell of the κ-decomposition of O, $0 \leq i \leq n$. The cell ϕ is included in some closed n-cube $\overline{\mathcal{C}}^n$ (Lemma 40) and its vertices are elements of $O \cap C^n$. Moreover the vertices of ϕ are κ-connected (Lemma 42), thus they are all 0-faces of an n-cell of $V_h(O, C^n)$. The open convex hull of these vertices, i.e., ϕ, is thus included in $\|V_h(O, C^n)\|$. Proposition 21 prevents the cell ϕ to meet any cell of $V_h(O, C^n)$ that is part of $\mathfrak{B}K_h(O)$. Because this statement is true for all n-cubes that contain ϕ, ϕ does not intersect the set $\mathfrak{B}K_h(O)$.

Let ψ be any j-cell of the λ-decomposition of Q. The case $n = 2$ is readily proven because $\{\kappa, \lambda\}$ is proper. Suppose $n \geq 3$. Since κ is quasi-complete, λ must be equal to ω_n (Lemma 8). The cell ψ is therefore a j-cube whose vertices are not in O. Let $\overline{\mathcal{C}}^n$ be a closed n-cube that contains ψ. If the corresponding digital n-cube meets O, let π be a cell of $V_h(O, C^n)$. The vertices of π are all included in $\overline{\mathcal{C}}^n \setminus \overline{\psi}$. Since the set $\overline{\mathcal{C}}^n \setminus \overline{\psi}$ is convex and π is the open convex hull of its vertices, $\pi \subset \overline{\mathcal{C}}^n \setminus \overline{\psi}$, which concludes the proof. □

We shall now demonstrate that the boundary of the solid extension has no boundary, i.e., it is a "closed" (hyper-)surface:

Lemma 23. Any $(n-2)$-cell of $\mathfrak{B}K_h(O)$ is the face of exactly two $(n-1)$-cells of $\mathfrak{B}K_h(O)$. Moreover any $(n-2)$-cell of $\mathfrak{B}K_h(O)$ is a subset of either an n-cube or a $(n-1)$-cube.

Proof. Let π^{n-2} be a $(n-2)$-cell of $\mathfrak{B}K_h(O)$. The demonstration is performed by cases, whether the $(n-2)$-cell π^{n-2} lies in an open n-cube, in an open $(n-1)$-cube or in a closed

$(n-2)$-cube (the latter is proved to be impossible).

If this cell is contained in an open n-cube $\mathcal{C}^n$, then it is a $(n-2)$-face of exactly one n-cell of $K_h(O)$, say π^n. Since the boundary of a closed polyhedral domain is a closed $(n-1)$-pseudomanifold (Lemma 50), the cell π^{n-2} is the face of exactly two $(n-1)$-cells of π^n. These $(n-1)$-cells must be in $\mathfrak{B}K_h(O)$. Indeed, if this was not the case, Lemma 18 would entail that they are included in some closed $(n-1)$-cube: since π^{n-2} lies in the closure of these cells, π^{n-2} should lie in this closed $(n-1)$-cube, which is a contradiction to the hypothesis.

Assume now that π^{n-2} is included in some $(n-1)$-cube $\mathcal{C}^{n-1}$. Then π^{n-2} is incident to one $(n-1)$-cell σ^{n-1} of $V_h(O, C^{n-1})$. From Lemma 14, σ^{n-1} is incident to exactly two n-cells of $K_h(O)$, say π_1^n and π_2^n, with π_1^n in an n-cube $\mathcal{C}_1^n$ and π_2^n in an n-cube $\mathcal{C}_2^n$. The $(n-2)$-cell π^{n-2} is incident to π_1^n by the $(n-1)$-cell σ^{n-1} and must be a face of another $(n-1)$-cell of π_1^n, say π_1^{n-1} (Lemma 50). As well, π^{n-2} is the face of another $(n-1)$-cell of π_2^n, say π_2^{n-1}. Because σ^{n-1} is already a subset of $\mathcal{C}^{n-1}$, $\pi_1^{n-1} \subset \mathcal{C}_1^n$ and $\pi_2^{n-1} \subset \mathcal{C}_2^n$, Lemma 18 implies that both π_1^{n-1} and π_2^{n-1} belong to $\mathfrak{B}K_h(O)$ and that σ^{n-1} does not belong to $\mathfrak{B}K_h(O)$. It is obvious that π^{n-2} cannot be incident to another n-cell of $K_h(O)$ hence to another $(n-1)$-cell.

Finally, suppose π^{n-2} is included in some closed $(n-2)$-cube $\overline{\mathcal{C}}^{n-2}$. We show that this case cannot occur by contradiction. This $(n-2)$-cube is shared by exactly four closed n-cubes, say $\overline{\mathcal{C}}_i^n$ with $0 \leq i \leq 3$. We organize them by adjacent pairs such that $\overline{\mathcal{C}}_i^n \cap \overline{\mathcal{C}}_{i+1}^n = \overline{\mathcal{C}}_i^{n-1}$, indices taken modulo 4. The cell π^{n-2} is incident to exactly one $(n-1)$-cell π_i^{n-1} in each $\overline{\mathcal{C}}_i^{n-1}$ and to exactly one n-cell π_i^n in each $\overline{\mathcal{C}}_i^n$. For each i, we have $\pi^{n-2} \prec \pi_i^{n-1}$, $\pi^{n-2} \prec \pi_{i+1}^{n-1}$, and $\pi_i^{n-1} \prec \pi_i^n$ and $\pi_{i+1}^{n-1} \prec \pi_i^n$. Since π_i^n is a convex polyhedral domain, there is no other $(n-1)$-cell of π_i^n that is incident to π^{n-2} (Lemma 50). Because each π_i^{n-1} is the face of exactly two n-cells of $K_h(O)$, it does not belong to $\mathfrak{B}K_h(O)$ (by definition). Since no other n-cell is incident to π^{n-2}, the cells π_i^{n-1} were the only $(n-1)$-cells of $K_h(O)$ incident to π^{n-2}. Consequently, $\pi^{n-2} \notin \mathfrak{B}K_h(O)$, which contradicts the hypothesis. □

3.2.4 Continuous analog of a digital boundary

Until now, we have not used the set Q of the $\kappa\lambda$-boundary $\partial(O, Q)$ in the construction of its continuous analog. The influence of the set Q is introduced in this section. The following

lemma shows that each cell of $\mathfrak{B}K_h(O)$ can border only one λ-component of the 0-voxels in I. Any component of this complex is built on boundary vertices of one κ-component of 1-voxels (here O) and one λ-component of 0-voxel of I. This is the first lemma where the value of the voxels is used in the proof.

Lemma 24. There is no r-cell of $\mathfrak{B}K_h(O)$, $r \leq n-1$, such that some of its vertices are elements of $\mathcal{A}_h(O,Q)$ and some others are elements of $\mathcal{A}_h(O) \setminus \mathcal{A}_h(O,Q)$.

Proof. It is sufficient to prove this lemma for $r = n-1$. We prove it by contradiction. Assume there exists one $(n-1)$-cell σ of $\mathfrak{B}K_h(O)$ with a 0-cell $a \in \mathcal{A}_h(O,Q)$ and a 0-cell $a' \in \mathcal{A}_h(O) \setminus \mathcal{A}_h(O,Q)$. This cell belongs to at least one n-cube $\overline{\mathcal{C}}^n$ (say). There exist two ω_n-adjacent voxels u and v with $u \in O \cap C^n$ and $v \in Q \cap C^n$ and a is lying on the open segment $]uv[$. Similarly, a' is lying on an open segment $]u'v'[$ with $u' \in O \cap C^n$, $v' \in C^n$ and $v' \notin O \cup Q$, and $\omega_n(u', v')$.

Let R^{n-1} be the carrying plane of σ. R^{n-1} divides the space $\mathbb{R}^n$ in two connected half-spaces, H^+ and H^-. The cell σ is a face of a n-cell π in $V_h(O, C^n)$. Hence R^{n-1} is a supporting plane of π. Clearly, all the voxels of $O \cap C^n$ incident to π are located in the same half-space, say H^-: u and u' are in H^-. The open segments $]ua[$ and $]u'a'[$ are included in H^-. Since a and a' lie in $R^{n-1} = \overline{H^-} \setminus H^-$, both v and v' must be included in H^+.

We show now that we can build an ω_n-path from v to v' in $C^n \setminus O$. The complex $V_h(O, C^n)$ contains one or two n-cells (Lemma 10). Since $\{\kappa, \lambda\}$ is connecting and, by assumption, the set of 0-voxels of C^n is not λ-connected, the set of 1-voxels of C^n is κ-connected, hence $O \cap C^n$ is κ-connected. Consequently, there is only one n-cell in $V_h(O, C^n)$ and it is π. Furthermore, any voxel of $C^n \cap H^+$ must be a 0-voxel, and it is sufficient to build an ω_n-path from v to v' in $C^n \cap H^+$.

It is always possible to find a voxel $w \in C^n$ with $\omega_n(v, w)$ and $\|w - v'\|_1 = \|v - v'\|_1 - 1$. If $w \in H^+$, we have found a new element of the path we are building. Otherwise, $w \in H^-$ and $w - v$ correspond to a unit vector. The voxel w' defined from v' by the displacement $v - w$ is such that $\omega_n(v', w')$ and $\|w' - v\|_1 = \|v' - v\|_1 - 1$. Because this displacement is opposite to the displacement $w - v$, w' must be in H^+. By iterating this construction, we build an ω_n-path between v and v' such that all its elements are in H^+, hence in $C^n \setminus O$. Since $\omega_n \subset \lambda$, we have found a λ-path joining v and v' that lies in $C^n \cap H^+$: any voxel of this path is a 0-voxel. v is

a 0-voxel in Q so all the path is in Q and $v' \in Q$. This contradiction concludes the argument. $\square$

If we collect the cells of $\mathfrak{B}K_h(O)$ whose vertices are boundary vertices between O and Q in I, Lemma 24 implies that this collection is a subcomplex of $\mathfrak{B}K_h(O)$. Because $\partial(O,Q)$ is not empty, this subcomplex is a $(n-1)$-dimensional polyhedral complex. This subcomplex is denoted by $\mathfrak{B}_{|Q}K_h(O)$.

We define now the continuous analog of a digital boundary as:

Definition 25 (Continuous analog of a $\kappa\lambda$-boundary). The *continuous analog induced by h of a $\kappa\lambda$-boundary* $\Sigma = \partial(O,Q)$ is defined as the body of the complex $\mathfrak{B}_{|Q}K_h(O)$. It is denoted by $\mathcal{S}_h(O,Q)$. The complex $\mathfrak{B}_{|Q}K_h(O)$ is called *the complex of* $\mathcal{S}_h(O,Q)$. All points of $\mathcal{A}_h(O,Q)$ are included in $\mathcal{S}_h(O,Q)$.

This definition is implicitly dependent on the image where the set O and Q are defined: the value of every voxel of O (respectively, Q) in I must be 1 (respectively, 0). It is also dependent on the adjacencies κ and λ chosen for I.

Note that we have not proved yet that the complex of $\mathcal{S}_h(O,Q)$ is strongly connected. The following theorem establishes this property and highlights some immediate consequences:

Theorem 26. Suppose $\{\kappa,\lambda\}$ is proper and connecting, and κ is quasi-complete. The continuous analog induced by h of a $\kappa\lambda$-boundary $\Sigma = \partial(O,Q)$ is strongly connected and separates the space $\mathbb{R}^n$ into two disjoint domains: one of these domains contains the κ-volume of O, the other contains the λ-volume of Q.

Proof. We first divide the complex of the continuous analog $\mathcal{S}_h(O,Q)$ into its strongly connected components, say $K_1,\ldots,K_l$ with $l \geq 1$. Each K_i is a strongly connected $(n-1)$-dimensional polyhedral complex and each $(n-2)$-cell of K_i is a face of exactly two $(n-1)$-cells of K_i (Lemma 23). Any simplicial subdivision of each K_i is thus a closed $(n-1)$-pseudomanifold and $\|K_i\|$ separates $\mathbb{R}^n$ into two disjoint domains H_i^+ and H_i^- (Theorem 49). For clarity, we set $H_i^0 = \|K_i\|$. By Theorem 22, for any i, $1 \leq i \leq l$, the κ-volume of O is in one of these domains (say H_i^+). The same theorem implies that the λ-volume of Q is, for a given i, either entirely in the same domain H_i^+, or entirely in the other domain H_i^-.

We prove by contradiction that the λ-volume of Q is in H_i^-. Suppose it is in H_i^+. Let

a be a vertex of K_i. Since $a \in \mathcal{A}_h(O,Q)$, it lies on an open segment $]uv[$, where $u \in O$, $v \in Q$, and $\omega_n(u,v)$. Clearly, the segment $]ua[$ is a 1-cell of $K_h(O)$. Proposition 21 entails that this segment is not in $\mathfrak{B}K_h(O)$. The segment $]av[$ is not a 1-cell of $K_h(O)$, hence it is not in $\mathfrak{B}K_h(O)$. Consequently, we have $\mathcal{S}_h(O,Q) \cap]uv[= \{a\}$. The hypothesis implies $[ua[\subset H_i^+$ and $]av] \subset H_i^+$ (with $a \in H_i^0$).

It is easy to see that the 0-cell a is the face of 2^{n-1} $(n-1)$-cells of the complex of $\mathcal{S}_h(O,Q)$. All these cells are strongly connected and are thus part of the same strongly connected component, i.e., K_i. Locally around a, the body of K_i is homeomorphic to a topological disk. Therefore, for a sufficiently small neighborhood V of a in $\mathbb{R}^n$, the set $H_i^+ \cap V$ is connected by arcs. Further, for a sufficiently small neighborhood V of a in $\mathbb{R}^n$, we have $H_j^0 \cap V = \emptyset$ for any $j \neq i$, $1 \leq j \leq l$. We choose such a small neighborhood V. Let $x \in]ua[\cap V$ and $y \in]av[\cap V$. Clearly, $x \in H_i^+ \cap V$ and $y \in H_i^+ \cap V$. Since $H_i^+ \cap V$ is connected by arcs, there exists an arc c from x to y included in $H_i^+ \cap V$. We build an arc c', entirely included in H_i^+, by gluing the segment $[ux]$, the arc c from x to y, and the segment $[yv]$. Since V is not met by any H_j^0 for $j \neq i$, the arc c' has an empty intersection with $\mathcal{S}_h(O,Q)$. We have built an arc joining u to v which does not meet $\|\mathfrak{B}_{|Q}K_h(O)\|$, although $u \in \|K_h(O)\| \setminus \|\mathfrak{B}K_h(O)\|$ and $v \notin \|K_h(O)\|$. According to the definition of the boundary of a complex, this arc should meet another component of $\|\mathfrak{B}K_h(O)\|$. Because this arc is built locally between the κ-component O and the λ-component Q, this is clearly impossible.

We deduce that the λ-volume of Q is in H_i^-. Now, any arc from an element of O to an element of Q should meet all the set H_i^0 for $1 \leq i \leq l$. In the previous paragraphs, we have just shown that the arc $[uv]$ intersects only one strongly connected component of the complex of $\mathcal{S}_h(O,Q)$. Therefore the complex of $\mathcal{S}_h(O,Q)$ has only one strongly connected component ($l = 1$) and any simplicial subdivision of this complex is a closed $(n-1)$-pseudomanifold. All the other statements are trivially deduced from this one and from Theorem 49. □

Corollary 27. Any arc in $\mathbb{R}^n$ from a voxel of O to a voxel of Q intersects $\mathcal{S}_h(O,Q)$.

Theorem 26 shows that, by a local approach, we have constructed a (hyper-)surface in $\mathbb{R}^n$. This (hyper-)surface has several nice properties: it is a strongly connected $(n-1)$-dimensional compactum in $\mathbb{R}^n$; it separates embedding of 1-voxels from embedding of 0-voxels in the space;

if the binary image I is a gray-level image I' thresholded by the iso-value s, the continuous analog induced by the boundary mapping defined in Section 3.1 is a linear approximation of the iso-potential set of value s in I'. Section 5 will apply this construction method to extract closed triangulated iso-surfaces from gray-level images.

3.3 Continuous analog when λ is quasi-complete

We define the continuous analog of a $\kappa\lambda$-boundary of a binary image I when λ is quasi-complete as the continuous analog of the corresponding $\lambda\kappa$-boundary of its negative image I^-:

Definition 28 (Continuous analog of a $\kappa\lambda$-boundary, λ quasi-complete). Let I be a binary image and h a boundary mapping of I. Let O be a κ-connected component of 1-voxels in I and Q a λ-connected component of 0-voxels in I. When $\{\kappa, \lambda\}$ is proper and connecting and λ is quasi-complete, the *continuous analog induced by h of the $\kappa\lambda$-boundary $\partial(O, Q)$ of I* is defined as the continuous analog induced by h^- of the $\lambda\kappa$-boundary $\partial(Q, O)$ of I^-, where Q is a λ-connected component of 1-voxels in I^- and O is a κ-connected component of 0-voxels in I^-. It is similarly denoted by $\mathcal{S}_h(O, Q)$.

This definition is valid because $\kappa\lambda$-boundaries in a binary image I are $\lambda\kappa$-boundaries in its negative image I^-. All properties shown until now are still valid when λ is quasi-complete. In particular, the κ-volume of O is separated from the λ-volume of Q by $\mathcal{S}_h(O, Q)$. Definition 25 and Definition 28 imply that we can define a continuous analog of any $\kappa\lambda$-boundary of an image I, provided that $\{\kappa, \lambda\}$ is proper and connecting, and either κ or λ is quasi-complete.

4 Properties and applications

4.1 New Jordan pairs for n

This section highlights an important application of continuous analogs of digital boundaries: the extraction of new Jordan pairs for arbitrary n. We have the following theorem.

Theorem 29. Any proper and connecting pair of voxel adjacency $\{\kappa, \lambda\}$ is a Jordan pair for $n \geq 2$ if either κ or λ is quasi-complete. In particular, for $n \geq 3$ and κ quasi-complete, $\{\kappa, \omega_n\}$ is a Jordan pair for n.

Proof. From Definition 28, we can assume that κ is quasi-complete. We have to prove that every $\kappa\lambda$-boundary (say Σ) of every binary image I has the following property: any ω_n-path from a voxel of $II(\Sigma)$ to a voxel of $IE(\Sigma)$ exits through Σ. Let $\Sigma = \partial(O, Q)$ nonempty. It is sufficient to show that any ω_n-path, say Ω, from $u \in O$ to $v \in Q$ exits through Σ. The ω_n-path Ω draws an arc in $\mathbb{R}^n$ which is a connected set of segments (Proposition 4). Corollary 27 entails this arc intersects $\mathcal{S}_h(O, Q)$ in some point a. The point a is a boundary vertex of $\mathcal{A}_h(O, Q)$ and lies between two voxels u' and v', with $u' \in O$, $v' \in Q$, $\omega_n(u', v')$, and both u' and v' are consecutive voxels of Ω. If the voxel u' appears just before v' in Ω, then (u', v') is a boundary surfel included in Σ and Ω exits through Σ. If u' appears after v' in Ω, then the restriction of Ω to the voxels from u' to v is an ω_n-path, say Ω', from an element of O to an element of Q, which is shorter than Ω. It draws an arc in $\mathbb{R}^n$ that intersects $\mathcal{S}_h(O, Q)$. By iterating the argument used on Ω, we establish that any ω_n-path from O to Q exits through Σ. □

For such pairs $\{\kappa, \lambda\}$, the $\kappa\lambda$-boundaries of any image have "good" properties. The preceding theorem asserts that $\{8, 4\}$ is a Jordan pair for $n = 2$, that $\{18, 6\}$ and $\{26, 6\}$ are Jordan pairs for $n = 3$, but also that the adjacency pair symbolized by $\{\not\asymp, \not\asymp\}$ is a Jordan pair for $n = 2$ (also known as "6-adjacency"). On the other hand, we cannot assert a similar result for the $\{6, 14\}$ voxel adjacency pair of Ref. [15] and its n-dimensional generalization of Ref. [41], since none of these voxel adjacencies are quasi-complete. It is thus possible to find Jordan pairs whose voxel adjacencies are not quasi-complete.

4.2 Continuous analog of $\mathbb{B}(I)$

In this section, we assume that $\{\kappa, \lambda\}$ is proper and connecting, and that κ is quasi-complete. We relate the number of $\kappa\lambda$-boundaries bordering a κ-component O of 1-voxels to the number of connected components of the body of $\mathfrak{B}K_h(O)$ with the following proposition, which can be demonstrated easily:

Proposition 30. Let I be any binary image (with both 0-voxels and 1-voxels) and h any boundary mapping of I. Let O be any κ-connected component of 1-voxels in I. Let $Q_1, \ldots, Q_l$ be the l different λ-connected components of 0-voxels in I such that $\partial(O, Q_i)$ is not empty for any $1 \leq i \leq l$. Then the set $\|\mathfrak{B}K_h(O)\|$ has either l or $l + 1$ connected components.

The l connected components are the l continuous analogs induced by h of the $\kappa\lambda$-boundaries $\partial(O, Q_i)$. The last one may appear if O forms the border of the domain of I; in this case, this component is a $(n-1)$-dimensional parallepiped in $\mathbb{R}^n$ embracing the whole domain of the image I.

The following theorem shows that $\kappa\lambda$-boundaries and their corresponding continuous analogs are disjoint at the same time :

Theorem 31. Let $\partial(O, Q)$ and $\partial(O', Q')$ be two (nonempty) $\kappa\lambda$-boundaries of a binary image I with a boundary mapping h. Their continuous analogs induced by h are not disjoint if, and only if, $O = O'$ and $Q = Q'$.

Proof. We just have to prove that if $O \neq O'$ or if $Q \neq Q'$, their continuous analogs $\mathcal{S}_h(O, Q)$ and $\mathcal{S}_h(O', Q')$ are disjoint. Assume first $O = O'$. Then their respective complexes $\mathfrak{B}_{|Q}K_h(O)$ and $\mathfrak{B}_{|Q'}K_h(O)$ are subcomplexes of the polyhedral complex $\mathfrak{B}K_h(O)$. Lemma 24 implies that their respective 0-cells are disjoint. The bodies of the complexes $\mathfrak{B}_{|Q}K_h(O)$ and $\mathfrak{B}_{|Q'}K_h(O)$ are necessary disjoint. Suppose now $O \neq O'$. Let C^n be any digital n-cube. If only one of $O \cap C^n$ or $O' \cap C^n$ is nonempty, then $\mathcal{S}_h(O, Q) \cap \mathcal{S}_h(O', Q') \cap \overline{\mathcal{C}}^n$ is empty by construction. Suppose both are nonempty. Since κ is quasi-complete, the sets $O \cap C^n$ and $O' \cap C^n$ are both reduced to one voxel of C^n, and these two voxels are diagonally opposite in C^n. With an argument similar to the proof of Lemma 10, we also get that $\mathcal{S}_h(O, Q) \cap \mathcal{S}_h(O', Q') \cap \overline{\mathcal{C}}^n$ is empty. Because this is true for any closed n-cube, we have $\mathcal{S}_h(O, Q) \cap \mathcal{S}_h(O', Q') = \emptyset$. □

This theorem allows us to define:

Definition 32 ($\kappa\lambda$-continuous analog of $\mathbb{B}(I)$). The *$\kappa\lambda$-continuous analog induced by h of* $\mathbb{B}(I)$ is the disjoint union of the continuous analogs induced by h of all the $\kappa\lambda$-boundaries of I, minus the one arising when $U(I)$ forms the border of the domain of I (see Proposition 30). It is denoted by $\mathcal{S}_h^{\kappa\lambda}(\mathbb{B}(I))$. The *complex of* $\mathcal{S}_h^{\kappa\lambda}(\mathbb{B}(I))$ is the union of the complexes of each continuous analog determined by I. It is trivially a $(n-1)$-dimensional polyhedral complex.

If there are p different $\kappa\lambda$-boundaries in I, then the set $\mathcal{S}_h^{\kappa\lambda}(\mathbb{B}(I))$ has p (strongly) connected component (it is clear that at most one κ-component of 1-voxels in I can lie on the border of the domain of I). The converse is also true.

4.3 Adjacency between boundary surfels

Until now, no adjacency has been introduced between boundary surfels of an image. Hence $\kappa\lambda$-boundaries inside an image must be extracted by *scanning* the whole image, or at least the whole component of foreground voxels. It would be prudent to define an adjacency between boundary surfels such that, starting from a given boundary surfel (u, v) and following the adjacencies, we could extract the whole set of boundary surfels bordering the κ-component of 1-voxels containing u and the λ-component of 0-voxels containing v. This process is called *digital surface tracking*. It is more efficient than the scanning method because it can find a $\kappa\lambda$-boundary without explicitly computing the κ-component of $U(I)$ and the λ-component of $N(I)$ that define it. Several authors [5, 19, 24, 39] have proposed adjacencies between boundary surfels to extract the whole $\kappa\lambda$-boundary in the three-dimensional case. For an arbitrary n, several adjacencies between boundary surfels along with corresponding tracking algorithms are presented in [41]. Conversely, it is also possible to extract object and background components starting from boundaries [42].

An essential property that should have any adjacency between boundary surfels is that the connected components defined by this adjacency correspond to the $\kappa\lambda$-boundaries of the image, for some κ and λ. An important property of such adjacencies is that it must allow an efficient tracking of surfels: for instance the adjacency should be local (only "neighboring" surfels can be adjacent). Ideally, the most efficient adjacency would be the one which provides a Hamiltonian circuit over the set of boundary surfels of a $\kappa\lambda$-boundary. However, it is not a simple task to compute a Hamiltonian circuit over a graph, and not all graphs are Hamiltonian.

For any binary image I and a boundary mapping h from $\mathbb{B}(I)$ to $\mathbb{R}^n$, $\{\kappa, \lambda\}$ proper and connecting, either κ or λ quasi-complete, we define the binary relation $\sigma_{I,h}^{\kappa\lambda}$ on $\mathbb{B}(I)$ such as: the relation $\sigma_{I,h}^{\kappa\lambda}(t, t')$ holds, with $t = (u, v)$ and $t' = (u', v')$ boundary surfels of I, if the open segment $]h(u, v)h(u', v')[$ is a 1-cell of the complex of $\mathcal{S}_h^{\kappa\lambda}(\mathbb{B}(I))$. If $\sigma_{I,h}^{\kappa\lambda}(t, t')$, we say that the boundary surfel t is $\sigma_{I,h}^{\kappa\lambda}$-*adjacent* to the boundary surfel t'.

The following lemma is easily demonstrated. It shows that the $\sigma_{I,h}^{\kappa\lambda}$-adjacency is local:

Lemma 33. Let $t, t' \in \mathbb{B}(I)$, then $\sigma_{I,h}^{\kappa\lambda}(t, t')$ implies t and t' are subsets of some digital m-cube, with $2 \leq m \leq n$.

It means that we need to look at only a neighborhood around a boundary surfel to find its $\sigma_{I,h}^{\kappa\lambda}$-adjacent boundary surfels. The neighborhood is constituted of the 2^{n-1} digital n-cubes containing this boundary surfel. The transitive closure of the $\sigma_{I,h}^{\kappa\lambda}$-adjacency induces $\sigma_{I,h}^{\kappa\lambda}$-components in $\mathbb{B}(I)$, which have the following property:

Theorem 34. If $\{\kappa, \lambda\}$ is proper and connecting, and either κ or λ is quasi-complete, then every $\kappa\lambda$-boundary in every image I with any boundary mapping h of I is a $\sigma_{I,h}^{\kappa\lambda}$-component of $\mathbb{B}(I)$.

Proof. Let $\partial(O, Q)$ be a $\kappa\lambda$-boundary of I. Its continuous analog $\mathcal{S}_h(O, Q)$ is strongly connected (Theorem 26). The 0-cells of the complex of $\mathcal{S}_h(O, Q)$ (i.e., $\mathfrak{B}_{|Q}K_h(O)$) are the points of $\mathcal{A}_h(O, Q)$. The graph, say G_1, whose vertices are the 0-cells of $\mathcal{A}_h(O, Q)$ and whose arcs are the 1-cells of $\mathfrak{B}_{|Q}K_h(O)$, is connected (otherwise it would not be strongly connected). From the definition of $\sigma_{I,h}^{\kappa\lambda}$-adjacency, the graph, say G_2, whose vertices are the surfels of $\partial(O, Q)$ and whose arcs are the $\sigma_{I,h}^{\kappa\lambda}$-adjacencies, is isomorph to G_1. Hence G_2 is connected. Now, any element of $\mathbb{B}(I) \setminus \partial(O, Q)$ cannot be $\sigma_{I,h}^{\kappa\lambda}$-adjacent to any element of $\partial(O, Q)$, which entails that the set $\partial(O, Q)$ is a $\sigma_{I,h}^{\kappa\lambda}$-component of $\mathbb{B}(I)$. □

Assume now we choose the trivial boundary mapping g for every image. Let I_1 and I_2 be two binary images, C_1^n and C_2^n two digital n-cubes such that the values of the voxels of C_1^n in I_1 are the same as the values of the voxels of C_2^n in I_2. Clearly, the cells of the complex of $\mathcal{S}_h^{\kappa\lambda}(\mathbb{B}(I_1))$ within $\overline{\mathcal{C}}_1^n$ are the same as the cells of the complex of $\mathcal{S}_h^{\kappa\lambda}(\mathbb{B}(I_2))$ within $\overline{\mathcal{C}}_2^n$ (up to an integer translation vector). Consequently, the $\sigma_{I_1,g}^{\kappa\lambda}$-adjacencies within $\overline{\mathcal{C}}_1^n$ are identical to the $\sigma_{I_2,g}^{\kappa\lambda}$-adjacencies within $\overline{\mathcal{C}}_2^n$. The family $\sigma_g^{\kappa\lambda}$ of adjacencies $\sigma_{I,g}^{\kappa\lambda}$ can be entirely determined by examining all the different configurations of 1-voxels and 0-voxels that occur in a digital n-cube. In other words, this last remark together with Theorem 34 and Theorem 29 implies that the ordered triple $(\kappa, \lambda, \sigma_g^{\kappa\lambda})$ is a *Jordan triple for* n in the terminology of Udupa [41].

We have just shown that, for these $\{\kappa, \lambda\}$ and for any image I, we can build an adjacency between boundary surfels, so that, starting from an initial boundary element, we can extract a whole $\kappa\lambda$-boundary of I by tracking adjacencies. The family $\sigma_g^{\kappa\lambda}$ of adjacencies is not as efficient as the adjacencies proposed in [5] or in [15], but they are suitable for arbitrary n. One way to design more efficient adjacencies is to prune the graph of $\sigma_{I,g}^{\kappa\lambda}$-adjacencies. Therefore,

we propose two adjacencies derived from this adjacency, and we conjecture that they also give rise to Jordan triples.

The following binary relations on $\mathbb{B}(I)$ are not dependent on the boundary mapping h and their definition is purely (digital) topological:

Definition 35 ($\sigma_I^{\kappa\lambda}$-adjacency on $\mathbb{B}(I)$). Two boundary surfels t and t' of I are said to be $\sigma_I^{\kappa\lambda}$-*adjacent* iff they are $\sigma_{I,h}^{\kappa\lambda}$-adjacent for any boundary mapping h of I.

Definition 36 ($\tilde{\sigma}_I^{\kappa\lambda}$-adjacency on $\mathbb{B}(I)$). Two boundary surfels $t = (u, v)$ and $t' = (u', v')$ of I are said to be *weakly* $\sigma_I^{\kappa\lambda}$-*adjacent*, or $\tilde{\sigma}_I^{\kappa\lambda}$-*adjacent*, iff: (i) $\sigma_I^{\kappa\lambda}(t, t')$ and (ii) there is no 1-voxel other than u and u' in the smallest digital m-cube containing t and t' when $m \geq 3$.

Clearly, for any h, we have $\tilde{\sigma}_I^{\kappa\lambda} \subset \sigma_I^{\kappa\lambda} \subset \sigma_{I,h}^{\kappa\lambda}$.

Conjecture 37. If we denote by $\sigma^{\kappa\lambda}$ (respectively, $\tilde{\sigma}^{\kappa\lambda}$) the family of $\sigma_I^{\kappa\lambda}$-adjacencies (respectively, $\tilde{\sigma}_I^{\kappa\lambda}$-adjacencies) for all binary images I, then both $(\kappa, \lambda, \sigma^{\kappa\lambda})$ and $(\kappa, \lambda, \tilde{\sigma}^{\kappa\lambda})$ are Jordan triples for n (the latter implies the former).

The conjecture "$(\kappa, \lambda, \tilde{\sigma}^{\kappa\lambda})$ is a Jordan triple for n" would have an interesting application for tracking: given a surfel t in I, we look at a digital 2-cube that includes it; if this 2-cube contains another 1-voxel, then we follow the adjacencies within this 2-cube; otherwise, we look at a digital 3-cube including this 2-cube; if this 3-cube contains another 1-voxel, then we follow the adjacencies within this 3-cube; otherwise, we iterate this process until the digital n-cube. This process is more efficient than checking all $\sigma_I^{\kappa\lambda}$-adjacencies.

5 The 3D case

In this section, we describe the construction of continuous analogs of digital boundaries for $n = 3$ and we exhibit the equivalence between triangulated iso-surfaces and these continuous analogs. Analogous to the marching cube method [30], we show that a table of 256 configurations can be constructed to speed up the computation of the continuous analog of all the boundary surfels of the image. With this table, iso-surfaces with well-defined properties can be computed within any image. After that, we turn to adjacencies between boundary surfels and

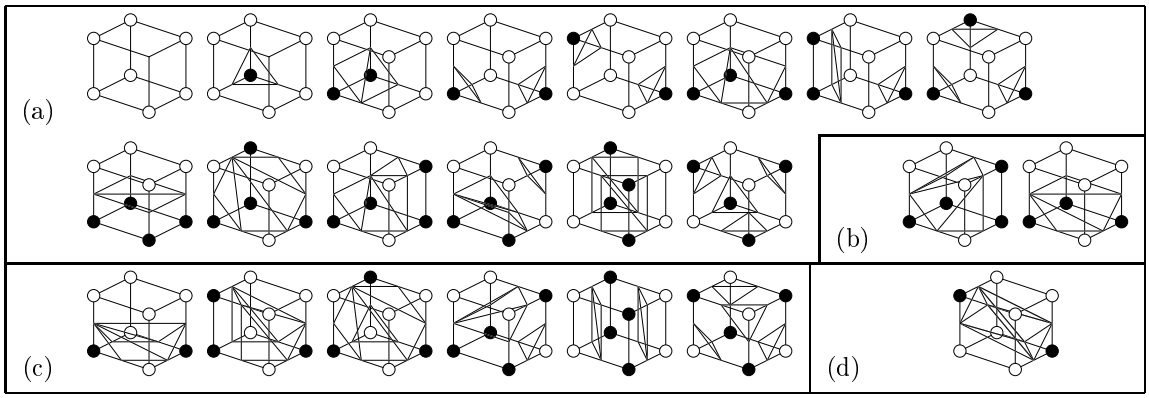

Figure 4: This figure displays the set of triangles associated with each noteworthy configuration (other configurations may be obtained from these via rotations or by taking the negative of the binary image) with the trivial boundary mapping. The 1-cells belonging to a face of a 3-cube, or *outer 1-cells* are displayed in thicker lines. The other 1-cells, or *inner 1-cells* are deduced from the convexity property of the local volume. Note that some 2-cells may be planar with more than three vertices. In this case, an arbitrary subdivision is performed. The pair (κ, λ) has an influence on the topology and on the geometry of the set of triangles: (a) triangles created when $\kappa = 6$, $\lambda \in \{18, 26\}$; (b) when $\lambda = 6$ and $\kappa \in \{18, 26\}$, these configurations have identical outer 1-cells as in (a) but the inner 1-cells are different; (c) when $\lambda = 6$ and $\kappa \in \{18, 26\}$, these configurations have different outer and inner 1-cells than in (a); (d) when $(\kappa, \lambda) = (26, 6)$, triangles are created to connect the opposite boundary vertices.

show that digital surface tracking algorithms can be used to construct triangulated iso-surfaces. We conclude by experimental results implementing our approach.

The ω_3-adjacency corresponds to 6-adjacency. The μ_3-adjacency corresponds to 18-adjacency and α_3 corresponds to 26-adjacency. Hence, the pairs $(26, 6)$, $(18, 6)$, $(6, 18)$, $(6, 26)$ are proper and connecting and one of the adjacency is quasi-complete. These pairs are also Jordan pairs for $n = 3$ (these statements have been demonstrated in [19, 32], but they also follow from Theorem 29). In the remainder of this section, we will deal with only these four tuples.

5.1 Configuration table

For a given boundary mapping h of I, Fig. 2 illustrates how to construct the continuous analog of $\mathbb{B}(I)$ inside a digital 3-cube. For each digital 3-cube included in the domain of I, a set of triangles is thus extracted. The whole set of triangles forms a closed triangulated surface in $\mathbb{R}^3$ which separates 1-voxels from 0-voxels.

Of course, even if this method of continuous analog construction is local, it is not very fast, because it requires to compute the convex hull of a dozen of points for each digital 3-cube of the domain of I. In order to avoid these repetitive computations, we can ignore in a first step the boundary mapping h of I and instead use the trivial boundary mapping g. With this assumption, if we take two different digital 3-cubes inside the domain of the image I with the same voxel values, the triangles built in either digital 3-cubes will be identical (up to a translation). Therefore, we can precompute the sets of triangles for each possible configuration of voxel values in a digital 3-cube. A table of 256 configurations is thus associated with each possible pair (κ, λ). Four tables are thus created, one for each element of $\{(26,6),(18,6),(6,18),(6,26)\}$.

Figure 4 shows the sets of triangles obtained for noteworthy configurations and highlights the dissimilarities between identical configurations but with different adjacencies. Clearly, they are similar to the 15 configurations introduced in [30] which were obtained with a rather *ad hoc* method. Here, the "ambiguity" of some configurations is naturally removed by the influence of the adjacencies. Any $\kappa\lambda$-continuous analog of $\mathbb{B}(I)$ for any binary image I is thus called a *$\kappa\lambda$-iso-surface of I*. Figure 5 emphasizes the variations between $\kappa\lambda$-iso-surfaces of the same binary image I when the pair (κ, λ) is changed. These variations reflect the variations in the $\kappa\lambda$-boundaries of this image.

Now, it would be interesting to allow the boundary vertices to move along their segment in order to obtain a "nicer" iso-surface. In fact, if we move the boundary vertices according to the boundary mapping h but on the triangles computed with the trivial boundary mapping, we obtain a surface that is very similar to the $\kappa\lambda$-continuous analog induced by h of $\mathbb{B}(I)$: these two surfaces are indeed homeomorphic. Figure 6 illustrates this method: the result is a linear approximation of the "continuous" iso-surface.

We have just described a method to quickly construct iso-surfaces[1] of an image I with a

[1] Note that we do not obtain exactly the $\kappa\lambda$-continuous analog of $\mathbb{B}(I)$, since the κ-volume of any κ-component

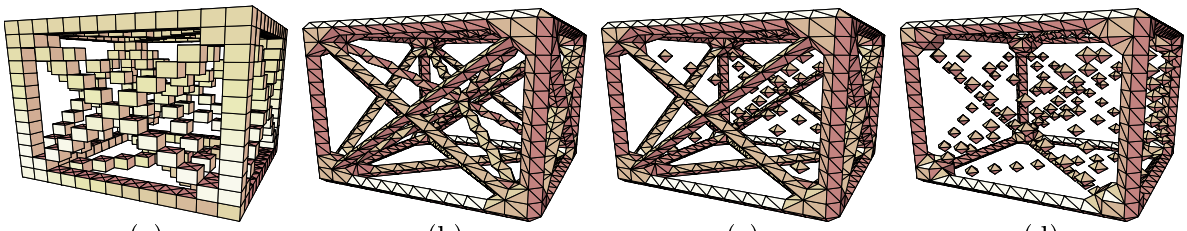

(a) (b) (c) (d)

Figure 5: The $\kappa\lambda$-iso-surfaces of a "connection" cube: (a) displays the binary image in block form; (b) $\kappa\lambda$-iso-surface with $(\kappa, \lambda) = (26, 6)$; (c) with $(\kappa, \lambda) = (18, 6)$; (d) with $(\kappa, \lambda) \in \{(6, 18), (6, 26)\}$.

boundary mapping h: (i) the first step uses one of the four trivial tables of configurations to obtain the topology of the triangulated surface; (ii) the second step moves vertices according to the boundary mapping h.

5.2 Transforming digital boundaries into iso-surfaces

In this section, we carry further what has been presented in Section 4.3 for the 3D case. We introduce the following binary relations between boundary surfels of binary images:

Definition 38 ($\beta_I^{\kappa\lambda}$-adjacency). Let $t_1 = (u, u')$ and $t_2 = (v, v')$ be two boundary surfels of an image I. These two surfels are said to be $\beta_I^{\kappa\lambda}$-*adjacent* if one of the statements below holds (see Fig. 7):

(i) $u = v$ and, either $\lambda(u', v')$ or the voxel w that is 6-adjacent to u' and to v' is a 0-voxel of I;

(ii) $u' = v'$ and, either $\kappa(u, v)$ or the voxel w that is 6-adjacent to u and to v is a 1-voxel of I;

(iii) u is 6-adjacent to v and u' is 6-adjacent to v';

(iv) $\kappa(u, v)$ and $\lambda(u', v')$, and, when $\kappa = 26$ (respectively, $\lambda = 26$), u and v (respectively, u' and v') are diagonally opposite voxels in the 3-cube containing t_1 and t_2, all other voxels of this 3-cube are 0-voxels of I (respectively, 1-voxels of I).

of 1-voxels and the λ-volume of any λ-component of 0-voxels may intersect this triangulated surface. We only have that their ω_n-volumes do not intersect the triangulated surface.

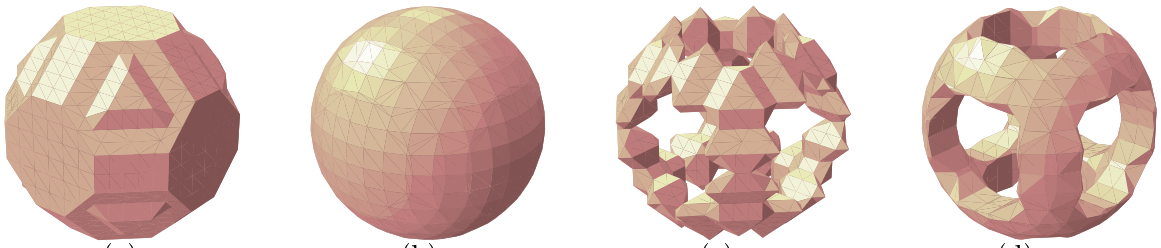

Figure 6: Visual comparison between boundary vertices mapped at the middle of their segment and boundary vertices mapped by the boundary mapping defined by the iso-value in the gray-level image (the image size is 15^3, the intensity value assigned to each voxel is the Euclidean distance to the image center, the surface normals are determined facet by facet as a vector product): (a) iso-surface of a sphere with the trivial boundary mapping; (b) same iso-surface with the non-trivial boundary mapping; (c) iso-surface of a sphere minus cylinders; (d) same iso-surface with the non-trivial boundary mapping. The complex defining the iso-surface (a) (respectively, (c)) is isomorph to the complex defining the iso-surface (b) (respectively, (d)).

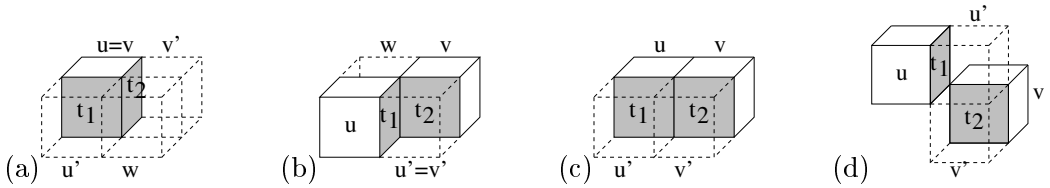

Figure 7: Illustration of the $\beta_I^{\kappa\lambda}$-adjacency relation between surfels of an image I: (a) point (i); (b) point (ii); (c) point (iii); (d) point (iv).

This adjacency relation induces a $\beta_I^{\kappa\lambda}$-connectedness relation and $\beta_I^{\kappa\lambda}$-components in $\mathbb{B}(I)$. The family of $\beta_I^{\kappa\lambda}$-adjacencies for all binary images I is denoted by $\beta^{\kappa\lambda}$.

For $(\kappa, \lambda) \in \{(18, 6), (6, 18)\}$, the relation $\beta_I^{\kappa\lambda}$ is the classical adjacency between boundary surfels that *share an edge* (i.e., two surfels *share an edge* if they are included in some digital 2-cube). This adjacency can be directed and an efficient algorithm has been developed to extract a $\beta_I^{18.6}$-component of $\mathbb{B}(I)$ (or a $\beta_I^{6.18}$-component of $\mathbb{B}(I)$) given a starting surfel [5]. In [19], it is shown that the extracted $\beta_I^{18.6}$-component of I (respectively, $\beta_I^{6.18}$-component of I) is a 18.6-boundary of I (resp 6.18-boundary of I). In other words, the triples $(18, 6, \beta^{18.6})$ and $(6, 18, \beta^{6.18})$ are Jordan triples for 3.

Point (iv) of this definition modifies the adjacencies when $\kappa = 26$ (or $\lambda = 26$): when O (or Q) is 26-connected but not 18-connected, it creates adjacencies betwen some surfels belonging to two different 18-components of O (or Q). More precisely, it creates adjacencies between surfels that are not sharing an edge (we say that these surfels are *sharing a vertex*). This point is compulsory since it has been demonstrated in [41] (Proposition 3.11) that 26.6-boundaries cannot be connected by an adjacency defined on boundary surfels sharing an edge in the general case.

By definition, the $\beta_I^{26.6}$-adjacency (respectively, $\beta_I^{6.26}$-adjacency) differs from the $\beta_I^{18.6}$-adjacency (respectively, $\beta_I^{6.18}$-adjacency) only on the digital 3-cubes containing two diagonally opposite 1-voxels (respectively, 0-voxels) and all others are 0-voxels (respectively, 1-voxels): we say that this 3-cube forms a *strict 26-configuration of 1-voxels* (respectively, *strict 26-configuration of 0-voxels*). Within this 3-cube, six additional relations are added to the relations defined by the $\beta_I^{18.6}$-adjacency. As far as we know, only the authors of [37] have added *one* adjacency between boundary surfels in the case of a strict 26-configuration (see Fig. 7d) and proved the validity of a surface tracking algorithm for these induced digital surfaces [2].

From any subset Σ of $\mathbb{B}(I)$ and any relation τ between elements of $\mathbb{B}(I)$, we define the *τ-surface graph of* Σ as the graph whose vertices are the surfels of Σ and whose arcs correspond to two surfels of Σ related by τ. It is denoted by $G(\Sigma, \tau)$. We have:

Proposition 39. Suppose $(\kappa, \lambda) \in \{(26, 6), (18, 6), (6, 18), (6, 26)\}$. Every $\kappa\lambda$-boundary in every binary image I is a $\beta_I^{\kappa\lambda}$-component of $\mathbb{B}(I)$ (i.e., $(\kappa, \lambda, \beta^{\kappa\lambda})$ is a Jordan triple for 3).

Proof. The cases $(\kappa, \lambda) \in \{(18, 6), (6, 18)\}$ has been demonstrated in [19]. For (26,6) (and (6,26)), we only sketch a demonstration: each 26-component is divided into its 18-components. On these 18-components the $\beta_I^{26.6}$-surface graph F (say) corresponds to the $\beta_I^{18.6}$-surface graph (which is connected). Every strict 26-configuration of 1-voxels induces $\beta_I^{26.6}$-adjacencies between bels of different $\beta_I^{18.6}$-components of F, thus connecting them together. We conclude by noticing that no other element of $\mathbb{B}(I)$ can be connected to F. □

It can be seen that, when $n = 3$, *the family $\beta^{\kappa\lambda}$ is identical to the family $\tilde{\sigma}^{\kappa\lambda}$* defined in

[2] This definition of adjacency is sufficient for a surface-tracking algorithm, where only one connection is required to extract 26.6-boundaries. However, this definition is not symmetrical and forbids subsequent properties.

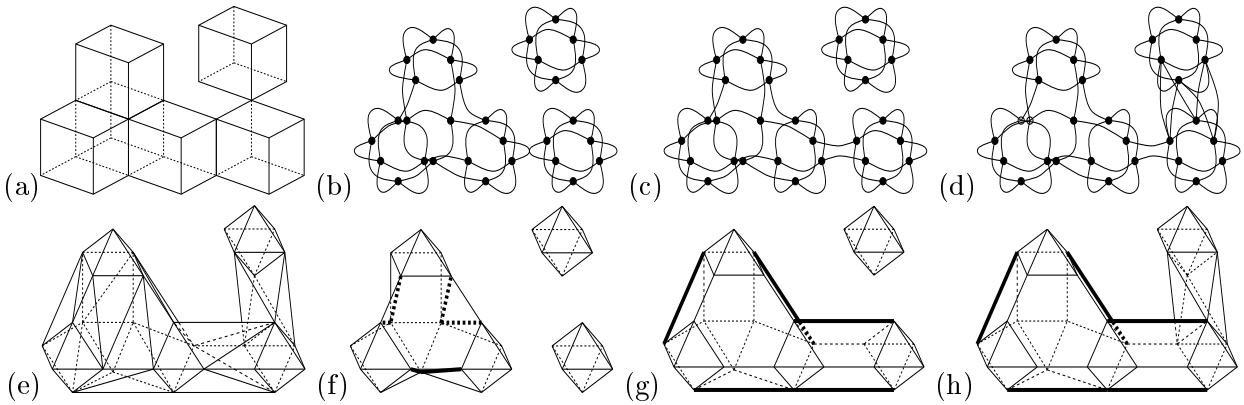

Figure 8: (a) Block representation of a binary image I; (b) the $\beta_I^{6.\lambda}$-surface graph of $\mathbb{B}(()I)$; (c) the $\beta_I^{18.6}$-surface graph of $\mathbb{B}(()I)$; (d) the $\beta_I^{26.6}$-surface graph of $\mathbb{B}(()I)$; (e) the 26.6-continuous analog of $\mathbb{B}(()I)$ displayed as a triangulated surface; (f) the $6.\lambda$-continuous analog of $\mathbb{B}(()I)$: the $\beta_I^{6.\lambda}$-adjacencies (or $\tilde{\sigma}_I^{6.\lambda}$-adjacencies) are the thin lines, the additional arcs defined by the $\sigma_I^{6.\lambda}$-adjacencies are the thick lines; (g) the 18.6-continuous analog of $\mathbb{B}(()I)$ with $\beta_I^{18.6}$-adjacencies in thin lines and additional $\sigma_I^{18.6}$-adjacencies in thick lines; (h) the 26.6-continuous analog of $\mathbb{B}(()I)$ with $\beta_I^{26.6}$-adjacencies in thin lines and additional $\sigma_I^{26.6}$-adjacencies in thick lines.

Section 4.3 [26]: informally, the relations coincide on each digital 2-cube and it can be verified that the local convex volume has the same six arcs in a strict 26-configuration. Conjecture 37 is thus valid for the 3D case. Figure 8 illustrates the analogy between the adjacencies between surfels and some 1-cells of the continuous analog. This figure also shows that the $\sigma_I^{\kappa\lambda}$-adjacency add arcs on the continuous analog which help to describe its geometry. However, the $\tilde{\sigma}_I^{\kappa\lambda}$-adjacency provides a sufficient description of the topology of the continuous analog.

In fact, a careful examination of Fig. 4 shows that, within any digital 3-cube, the restriction of the $\beta_I^{\kappa\lambda}$-surface graph of $\mathbb{B}(I)$ can be arranged into a set of oriented loops[3](refer to [25] for a demonstration). These loops can be oriented so that loops from adjacent digital 3-cubes

[3]More precisely, this surface graph is *representable* on the continuous analog (i.e., it can be drawn on this set so that no arcs intersect except at their endpoints). The continuous analog minus a representation of the surface graph defines connected sets. Each of these sets is homeomorphic to an open disc of the plane. Hence, the boundary of any of these connected elements can be delineated by a loop on the arcs of the surface graph. Note that the $\beta_I^{26.6}$-surface graph would not be representable on the 26.6-continuous analog without the point (iv) of the definition of $\beta_I^{\kappa\lambda}$-adjacency.

visit the same arc in opposite directions. Furthermore, it can be shown that the $\beta_I^{\kappa\lambda}$-surface graph of $\mathbb{B}(I)$ with these locally defined loops is a *2D combinatorial manifold without boundary* [11], which is the combinatorial analog of the 2-manifold without boundary. Each loop of the 2D combinatorial manifold can then be triangulated in order that the resulting triangulated manifold embedded into $\mathbb{R}^3$ by a boundary mapping h is exactly the $\kappa\lambda$-continuous analog induced by h of I.

From Fig. 4 it can be seen that any boundary surfel is incident to exactly one loop within a digital 3-cube except in the case of a strict 26-configuration, where the surfel is incident to three loops. Any surfel is included in exactly four digital 3-cubes. Therefore, we propose the following algorithm to transform the $\beta_I^{\kappa\lambda}$-surface graph of $\mathbb{B}(I)$ into the $\kappa\lambda$-continuous analog of $\mathbb{B}(I)$, which is restricted to the case $(\kappa, \lambda) \in \{(18, 6), (6, 18)\}$:

(Given an image I, a boundary mapping h, an empty mesh K)
For every surfel t in $G(\mathbb{B}(I), \beta_I^{\kappa\lambda})$
  For every digital 3-cube C containing t
    clear the flag (t, C)
EndFors
For every surfel t in $G(\mathbb{B}(I), \beta_I^{\kappa\lambda})$
  For every digital 3-cube C containing t
    If the flag (t, C) is not set
      – follow the two $\beta_I^{\kappa\lambda}$-adjacencies of t in C
        to extract the loop $L = (t_1, \ldots, t_l)$ in C containing t
      – triangulate L (convex hull computation or look-up in table)
      – add the vertices $h(t_i)$, edges and triangles to K
      – for all $i = 1..l$, set the flag (t_i, C).
    Endif
EndFors
Return K

The preceding algorithm can be extended to extract 26.6- or 6.26-boundaries by checking the number of $\beta_I^{\kappa\lambda}$-adjacencies of t in C. Furthermore, the topology of the mesh is naturally constructed by the $\beta_I^{\kappa\lambda}$-adjacencies.

We have just shown that a component of a $\kappa\lambda$-continuous analog of $\mathbb{B}(I)$ can be directly computed from the $\beta^{\kappa\lambda}$-adjacencies of the corresponding $\kappa\lambda$-boundary. A surface tracking algorithm (such as [5] for $\{18, 6\}$ or [37] for $\{26, 6\}$), which stores adjacencies between surfels, builds a surface graph of a $\kappa\lambda$-boundary in $O(q^2)$ time complexity, for an image of size q^3. The traversal of the surface graph has the same complexity. Now, the creation of new edges to triangulate the surface graph can be made in $O(1)$ around each surfel (simply by storing the different subdivision once and for all). *Consequently, the computation of a connected iso-surface can be done in* $O(q^2)$. It is a significant improvement to the marching cubes algorithm (whose time complexity is $O(q^3)$) when we do not need to compute the whole iso-surface of an image but only *one of its components*. Moreover, it shows that a digital surface can easily be transformed into an iso-surface and that the converse can also be realized.

5.3 Experimental results

We have implemented the algorithm which transforms the surface graph of a $\kappa\lambda$-boundary of an image I into the continuous analog of this $\kappa\lambda$-boundary. Note that this implementation is just a prototype and can be optimized by many ways. Figure 9 shows that this method for computing a connected iso-surface is less sensitive to the addition of pepper and salt noise than the classical scanning method. Moreover, the greater is the size of the image the slower is the scanning method compared to the transformation of the digital boundary. Of course, rather large data sets are needed to obtain a substantial gain with the tracking approach: this is due to the fact that the marching cubes algorithm "marches" very quickly on empty or filled digital 3-cubes and its theoretical complexity is not a very accurate description of its behavior when the image is rather "simple."

6 Conclusion

In this paper, we have proposed a new definition for the continuous analog of any digital boundary. The continuous analog is defined as an assembly of $(n-1)$-dimensional elements, which are computed within each digital n-cube meeting the digital boundary. We have proved that it is a $(n-1)$-dimensional polyhedron that separates the space into two disjoint domains.

It shares common topological properties with its corresponding digital boundary (separation of the space, connectedness). The Jordan–Brouwer separation theorem in the Euclidean space has entailed several significant digital topology results: new Jordan pairs for arbitrary n have been exhibited, and new families of adjacencies between elements of digital boundaries have been proposed. Furthermore, it has been shown that a continuous analog constitutes a piecewise approximation of some iso-potential set in a scalar field: it is a triangulated iso-surface of a volumetric dataset in the 3D case. The continuous analog can hence be used to compute implicitly defined (hyper-)surfaces with well-defined properties. The continuous analog definition shows that this polyhedron can be constructed either from its digital boundary or directly from the binary image. In the 3D case, we have shown how to transform a digital boundary with adjacencies into its continuous analog (i.e., a connected iso-surface) by a simple traversal of the surface graph of this digital boundary. A classical digital surface tracking algorithm can thus be used to build a triangulated iso-surface.

In the future, we plan to pursue our study of the topological and geometrical properties of continuous analogs. Recent works [6] show that the continuous analog of a three-dimensional boundary satisfies the Delaunay constraint: for instance, this geometric characteristic is fundamental in the construction of volumetric meshes for finite-element methods. We intend to verify whether this property holds for further dimensions. We are also working on methods to derive boundary surfel adjacencies from the definition of continuous analog, so that the digital boundaries are efficiently tracked and transformed into continuous analogs.

Acknowledgments

The authors thank Jean-Marc Nicod and Serge Miguet for providing a parallel version of the Marching-Cubes algorithm. Tests on real data were performed by this algorithm with modified configuration tables. The authors are also grateful to Vincent Bouchitté, Denis Richard, and Jayaram K. Udupa for helpful comments and discussions, and to Guillaume Berche and Nadège Saint Martin Tillet for their careful rereading. The authors also thank the anonymous reviewers for their valuable and constructive comments.

A Notation conventions

Throughout the paper, some symbols and letters are preferred to designate specific sets: n is the dimension of the spaces we are dealing with ($\mathbb{Z}^n$ and $\mathbb{R}^n$), the lowercase letters i, j, k, l, m, p, q, r denote integer numbers, the letter s is an iso-value, the letters f, g, h denote mappings, I and J are images or binary images, subsets of $\mathbb{Z}^n$ are uppercase letters (generally A, B, O, Q) sometimes with a superscript letter (digital m-cube C^m), elements of $\mathbb{Z}^n$ (voxels) are symbolized by lowercase letters (generally c, d, e, u, v, w), subsets of $\mathbb{R}^n$ or aggregates of subsets of $\mathbb{R}^n$ (except complexes and graphs) are denoted by uppercase calligraphic letters ($\mathcal{A}, \mathcal{D}, \mathcal{G}$) sometimes with a superscript (m-cube $\mathcal{C}^m$), points of $\mathbb{R}^n$ are denoted like voxels except that the letter a always designates a boundary vertex, complexes are generally denoted by K and graphs by G, the greek letters π, ϕ, ψ symbolize simplices and convex polyhedral domains (often with a superscript denoting its dimension), the greek letters $\rho, \kappa, \lambda, \omega, \eta, \mu, \alpha$ designate adjacency relations between voxels, the greek letter σ, β, τ designates adjacency relations between surfels, the uppercase greek letters Ω, Λ indicate sequences such as paths or chains, the greek letter Σ designates a digital surface. In any case, the addition to a symbol of a prime, of subscripts, or of parameters do not modify the semantic of this symbol.

B m-dimensional convex sets

The Euclidean n-dimensional space is denoted by $\mathbb{R}^n$. A r-dimensional subspace of $\mathbb{R}^n$, $0 \leq r \leq n$ is called a r-dimensional plane of $\mathbb{R}^n$ or simply *r-plane*. If $a_0, \ldots, a_r$ are $r+1$ linearly independent points of $\mathbb{R}^n$, they define a unique r-plane going through these points.

A set $\mathcal{M}$ of points of the Euclidean space $\mathbb{R}^n$ is said to be *convex* if it contains with every two of its points a and b the whole segment $[ab]$. The intersection of an arbitrary number of convex sets is convex. The *dimension number* of a convex set $\mathcal{M}$ is, by definition, the maximum number r such that $\mathcal{M}$ contains $r+1$ linearly independant points. Since it corresponds to the *topological dimension*, we will rather use the term *dimension*. Every convex set $\mathcal{M}$ of dimension r is contained in a uniquely defined r-plane, the *carrying plane* of $\mathcal{M}$, and it contains interior points with respect to this plane. Unless otherwise specified, interior points of a convex set $\mathcal{M}$ always refers to interior points of $\mathcal{M}$ *relative to its carrying plane*. The *closure* of $\mathcal{M}$, denoted

by $\overline{\mathcal{M}}$, is the smallest closed set containing $\mathcal{M}$. The *boundary* of $\mathcal{M}$, denoted by $\delta\mathcal{M}$, is defined as the closure of $\mathcal{M}$ minus its interior (relative to its carrying plane).

The *closed convex hull* of a set $\mathcal{M} \subset \mathbb{R}^n$ is defined as the intersection of all the convex sets containing $\mathcal{M}$ and is denoted by $\mathrm{Conv}(\mathcal{M})$. The closed convex hull of a finite set of points $a_0, \ldots, a_k$ consists of all the points $a \in \mathbb{R}^n$ of the form $a = \gamma_0 a_0 + \cdots + \gamma_k a_k$, where $\gamma_0, \ldots, \gamma_k$ are arbitrary nonnegative real numbers whose sum is 1. The *open convex hull* of a finite set of points $a_0, \ldots, a_k$ is the subset of the closed convex hull of $a_0, \ldots, a_k$ obtained by restricting the coefficients $\gamma_0, \ldots, \gamma_k$ to be strictly positive. The open convex hull of a finite set of points is open relative to its carrying plane. The set of *extremal points* of a convex set $\mathcal{M}$ is defined as the set of points $b \in \mathcal{M}$ such that $\mathcal{M} \setminus b$ is still convex. It is denoted by $\mathrm{Extr}(\mathcal{M})$.

Let $e_0, \ldots, e_r$, $0 \leq r \leq n$, be $r+1$ linearly independent points in the Euclidean space $\mathbb{R}^n$. The open convex hull of these points is called a *Euclidean r-simplex* of vertices $e_0, \ldots, e_r$. These vertices form the skeleton of the r-simplex. A p-simplex π is a *face* (or more specifically a *p-face*) of the r-simplex π' if the skeleton of π is a subset of the skeleton of π'. Obviously, $p \leq r$. A face π of π' is *proper* when $\pi \neq \pi'$. Any proper face of π is included in $\overline{\pi} \setminus \pi$. The set of extremal points of the closure of any simplex π coincides with its skeleton (i.e. the set of its 0-faces). We will often use the superscript notation π^m to indicate that the simplex π^m is m-dimensional.

A bounded nonempty subset of $\mathbb{R}^n$ which is the intersection of a finite number of open (closed) half-spaces of $\mathbb{R}^n$ is called a *convex polyhedral domain* (*closed polyhedral domain*). We use the same superscript notation for convex polyhedral domain as for simplices. Let ϕ^n be a n-dimensional convex polyhedral domain. If R^{n-1} is a $(n-1)$-plane in $\mathbb{R}^n$, such that $\overline{\phi^n} \cap R^{n-1} \neq \emptyset$ and $\phi^n \cap R^{n-1} = \emptyset$, then R^{n-1} is called a *supporting plane* of ϕ^n. The intersection of any supporting plane with the boundary $\overline{\phi^n} \setminus \phi^n$ of ϕ^n is a closed polyhedral domain $\overline{\phi^r}$, $r \leq n-1$; if $r = n-1$, ϕ^r is called a $(n-1)$-face of the polyhedral domain ϕ^n. Furthermore the $(n-2)$-faces of the $(n-1)$ faces of ϕ^n are called the $(n-2)$-faces of ϕ^n, etc. It can be demonstrated that every two faces of a convex polyhedral domain are disjoint and that the union of all the r-faces of ϕ^n, $0 \leq r \leq n-1$, is the boundary $\overline{\phi^n} \setminus \phi^n$. The set ϕ^n is itself called the *n-face* of ϕ^n. The other faces of ϕ^n are said to be *proper*. The 0-faces of ϕ^n are exactly the extremal points of $\overline{\phi^n}$.

C Continuous analogs of voxels

This section establishes the equivalence between the ρ-connectedness of a set A in the space $\mathbb{Z}^n$ and the connectedness of the ρ-1-skeleton of A in the space $\mathbb{R}^n$. For the case $n = 3$, we show that this connectedness is also equivalent to the connectedness of the ρ-volume of A in $\mathbb{R}^3$. In this section, ρ is an adjacency between voxels, A designates a set of voxels that is not empty.

The following lemma comes from the fact that any adjacency relation ρ includes the adjacency ω_n; therefore, point (ii) of Definition 2 and the minimal property of cells entails finer aggregates; the uniqueness comes from the fact that $\mathcal{G}_{\omega_n}(\mathbb{Z}^n)$ forms a partition of $\mathbb{R}^n$.

Lemma 40. Any i-cell ϕ of $\mathcal{G}_\rho(\mathbb{Z}^n)$, $0 \leq i \leq n$, is included in exactly one j-cell of $\mathcal{G}_{\omega_n}(\mathbb{Z}^n)$, $i \leq j \leq n$. This cubical cell is called the *enclosing cell* of ϕ.

Note that in the previous lemma we cannot substitute ω_n with any adjacency relation ρ' included in ρ (a simple counterexample is the 6- and the 8-adjacency in $\mathbb{Z}^2$). Lemma 40 induces:

Lemma 41. If any two cells of $\mathcal{G}_\rho(\mathbb{Z}^n)$ have a nonempty intersection, then they have the same enclosing cell.

The next lemma is trivially obtained:

Lemma 42. Let $\phi \in \mathcal{G}_\rho(A)$. Then the set of the vertices of ϕ is ρ-connected.

We will need the two following lemmas:

Lemma 43. Let ϕ be an i-cell of $\mathcal{G}_\rho(A)$. If ϕ has a nonempty intersection with a 1-cell ψ of $\mathcal{G}_\rho(A)$ then the set gathering the vertices of ϕ and the vertices of ψ is ρ-connected.

Proof. From Lemma 41, ϕ and ψ share the same enclosing cell C. This cell is bordered by k voxels $a_1, \ldots, a_k$. Since ψ is an open segment in C, it must be a main diagonal of C; Lemma 42 implies that the two vertices of ψ are ρ-adjacent and are diagonally opposite voxels of C. Point (iv) of the adjacency relation definition induces that any a_j, $1 \leq j \leq k$, is ρ-adjacent to the two vertices of ψ. Since each vertex of ϕ is in $\{a_1, \ldots, a_k\}$, it concludes the proof. □

Lemma 44. Assume $n \leq 3$. If ϕ is an i-cell of $\mathcal{G}_\rho(A)$, $i \geq 2$, and ψ is a j-cell of $\mathcal{G}_\rho(A)$, $j \geq 2$,

and $\phi \cap \psi \neq \emptyset$, then there exist two elements of $\mathcal{G}_\rho(A)$, say ϕ' and ψ', such that ϕ' is an i'-cell, ψ' is a j'-cell, $\phi' \cap \psi' \neq \emptyset$, $\phi' \subset \overline{\phi}$, $\psi' \subset \overline{\psi}$, and either $i' < i$ or $j' < j$.

Proof. We build these two elements to prove this statement. Let ϕ and ψ be two elements following the hypothesis. The set $\phi \cap \psi$ is not empty. According to a classical result of analytic geometry,[4] the dimension of this convex set is at least 1-dimensional. Therefore, the set $\delta(\phi \cap \psi)$ is also not empty. Let y be a point of this set. Then, either $y \in \delta\phi$ or $y \in \delta\psi$. In the first case, y belongs to an i'-cell ϕ' of $\mathcal{G}_\rho(A)$ with $i' < i$, and y obviously belongs to $\overline{\psi}$, hence to a j'-cell of $\mathcal{G}_\rho(A)$, $j' \leq j$, included in $\overline{\psi}$, say ψ'. The second case is symmetric to the first case. □

We can now demonstrate the following proposition (Proposition 4 of Section 2.3:

Proposition 45. The three following statements are equivalent when $n \leq 3$, if A is a finite set of voxels and ρ an adjacency relation:

(i) the set A is ρ-connected,

(ii) the ρ-1-skeleton of A is connected,

(iii) the ρ-volume of A is connected.

Proof. From the definition of ρ-decomposition, it is obvious that (i) ⇒ (ii). Now (ii) ⇒ (iii) because for any i-cell ϕ of the ρ-decomposition of A, $2 \leq i \leq n$, $\overline{\phi}$ contains some 1-cells; the Hausdorff-Lennes separation condition, i.e. $(\overline{A} \cap B) \cup (A \cap \overline{B}) = \emptyset$, concludes the argument.

To prove (iii) ⇒ (i), we show that we can construct a ρ-path in A between any two voxels a, b of A. Let $\{\phi_i\}$ be all the elements of $\mathcal{G}_\rho(A)$. Since the ρ-volume of A is connected, there exists a sequence $\overline{\phi_{i_0}}, \ldots, \overline{\phi_{i_k}}$ such that $\phi_{i_0} = a$, $\phi_{i_k} = b$, and $\overline{\phi_{i_j}} \cap \overline{\phi_{i_{j+1}}} \neq \emptyset$ for $0 \leq j < k$.

For any $0 \leq j < k$, if $\overline{\phi_{i_j}}$ and $\overline{\phi_{i_{j+1}}}$ meet on one of their vertices (hence a voxel), then Lemma 42 induces that the set of vertices of $\overline{\phi_{i_j}}$ and the set of vertices of $\overline{\phi_{i_{j+1}}}$ are both ρ-connected. Since these two sets have one vertex in common, their union is ρ-connected.

[4] The intersection of two planes, one i-dimensional and the other j-dimensional, in the space $\mathbb{R}^n$ is either empty or is a d-dimensional plane, $d \geq i + j - n$. Now, ϕ is open in its carrying i-plane, ψ is open in its carrying j-plane, the set $\phi \cap \psi$ is thus open in its carrying d-plane. When $n \leq 3$, the hypothesis implies $d \geq 1$. For higher dimensions, the set $\phi \cap \psi$ might be an isolated point in $\mathbb{R}^n$, and we cannot use this argument to conclude.

If $\overline{\phi_{i_j}}$ and $\overline{\phi_{i_{j+1}}}$ do not meet on one of their vertices, then they intersect on their interior. Thus ϕ_{i_j} (resp. $\phi_{i_{j+1}}$) is a k-cell (resp. l-cell) of $\mathcal{G}_\rho(A)$, with $k \geq 1$ and $l \geq 1$. If both $k > 1$ and $l > 1$, then the iteration of Lemma 44 induces that there exist two elements of the ρ-decomposition of A, say ψ_1 and ψ_2, with $\psi_1 \cap \psi_2 \neq \emptyset$, such that one of them is a 1-cell and $\psi_1 \subset \phi_{i_j}$ and $\psi_2 \subset \phi_{i_{j+1}}$. If either $k = 1$ or $l = 1$, we take $\psi_1 = \phi_{i_j}$ and $\psi_2 = \phi_{i_{j+1}}$. According to Lemma 43, the set of the vertices of ψ_1 and of the vertices of ψ_2 is ρ-connected. Lemma 42 induces that the set of vertices of ϕ_{i_j} is ρ-connected and that the set of vertices of $\phi_{i_{j+1}}$ is also ρ-connected. Since the vertices of ψ_1 (resp. the vertices of ψ_2) are also vertices of ϕ_{i_j} (resp. vertices of $\phi_{i_{j+1}}$), the set of the vertices of ϕ_{i_j} and of the vertices of $\phi_{i_{j+1}}$ is ρ-connected.

We have just built a chain of voxels of A between a and b, such that two successive sets of voxels are ρ-connected. Hence, there exists a ρ-path in A between any two voxels of A. □

For arbitrary n, it is easy to see from the preceding proof that (i) and (ii) are always equivalent and that (i) or (ii) implies (iii). The whole Proposition 4 is also true for the adjacency relations α_n and ω_n in arbitrary dimension n.

D Complexes, Pseudomanifolds

This section recalls classical definitions and theorems of combinatorial topology [2, 28].

Definition 46 (strongly connected m-complex). An m-dimensional complex K is said to be *strongly connected* if every two m-simplices (or m-cells) can be connected by a chain of m-simplices (or m-cells) such that any two consecutive simplices have a $(m-1)$-dimensional face in common. The body of a strongly connected complex cannot be separated by any closed set of dimension $\leq m-2$. The strong connectedness is part of the definition of pseudomanifolds (see below).

Definition 47 (subdivision of a complex). A *subdivision of the complex K* is any polyhedral complex K' such that (i) the body of K' coincides with the body of K and (ii) every element of the complex K', considered as a point set, is contained in some element of the complex K. A *simplicial subdivision* of a complex K is a subdivision K' the elements of which are simplices. Every polyhedral complex numbers Euclidean complexes among its subdivisions. It is a well

known result that a complex and any of its subdivisions have identical topological properties.

The following definition provides a multidimensional analog to the notion of "surface." The term "simple geometric n-circuit" has been preferred by some authors [28] to the term "pseudomanifold."

Definition 48 (m-pseudomanifold). A strongly connected (finite) m-dimensional Euclidean complex K is called a *m-pseudomanifold* if every $(m-1)$-simplex of K^m is a face of one or two m-simplexes. The subcomplex of K consisting of all the faces (proper or not) of the $(m-1)$-simplexes of K which are faces of precisely one m-simplex of K is referred to as the *boundary* of K, denoted by $\mathfrak{B}K$. If $\mathfrak{B}K$ is null, then K is said to be *closed*, otherwise K is said to be *with boundary*.

These complexes are particularly interesting because, for $m = n-1$, they separate the space $\mathbb{R}^n$ in two connected parts as it is stated by the following theorem [2]:

Theorem 49 (Jordan–Brouwer). Every closed $(n-1)$-pseudomanifold in $\mathbb{R}^n$ is orientable, separates $\mathbb{R}^n$ into precisely two domains, and is the common boundary of these two domains.

The following lemma will be useful in some demonstrations.

Lemma 50. Let X be an n-dimensional convex polyhedral domain in $\mathbb{R}^n$, K the polyhedral complex made of X and its faces. K is an n-pseudomanifold with boundary. Its boundary $\mathfrak{B}K$ is a closed $(n-1)$-pseudomanifold.

References

[1] R. Aharoni, G. T. Herman, and M. Loebl. Jordan graphs. *Graphical Models and Image Processing*, 58(4):345–359, July 1996.

[2] P. S. Aleksandrov. *Combinatorial Topology*. Graylock Press, Baltimore, MD, 1960.

[3] E. L. Allgower and S. Gnutzmann. Simplicial pivoting for mesh generation of implicitly defined surfaces. *Computer Aided Geometric Design*, 8:305–325, 1991.

[4] E. L. Allgower and P. H. Schmidt. An algorithm for piecewise linear approximation of an implicitly defined manifold. *SIAM Journal of Numerical Analysis*, 22:322–346, 1985.

[5] E. Artzy, G. Frieder, and G.T. Herman. The theory, design, implementation and evaluation of a three-dimensional surface detection algorithm. *Computer Graphics and Image Processing*, 15:1–24, 1981.

[6] D. Attali and J.-O. Lachaud. Constructing iso-surfaces satisfying the Delaunay constraint; application to the skeleton computation. In *Proc. 10th Int. Conf. on Image Analysis and Processing (ICIAP'99), Venice, Italy, Sept. 27-29*, pages 382–387, 1999.

[7] J. Bloomenthal. Polygonalization of implicit surfaces. *Computer Aided Geometric Design*, 5:341–355, 1988.

[8] J. Bloomenthal. *Introduction to Implicit Surfaces*, chapter 4, pages 126–165. Computer Graphics and Geometric Modeling series. Morgan Kaufmann Publishers, Inc., San Francisco, California, 1997.

[9] J.-H. Chuang and W.-C. Lee. Efficient Generation of Isosurfaces in Volume Rendering. *Computer & Graphics*, 19(6):805–813, 1995.

[10] H.E. Cline, C.R. Crawford, W.E. Lorensen, S. Ludke, and B.C. Teeter. Two algorithms for the three-dimensional reconstruction of tomograms. *Medical Physics*, 15(3), May 1988.

[11] J. Françon. Discrete Combinatorial Surfaces. *CVGIP: Graphical Models and Image Processing*, 57(1):20–26, January 1995.

[12] P.J. Frey and H. Borouchaki. Texel: triangulation de surfaces implicites. partie I: aspects théoriques. Research Report 3066, INRIA, Rocquencourt, France, December 1996.

[13] D. G. Gadian. *NMR and its application to Living systems.* Oxford Univ. Press., Oxford, UK, 1982.

[14] A. Van Gelder and J. Wilhelms. Topological Considerations in Isosurface Generation. *ACM Transactions on Graphics*, 13(4):337–375, October 1994.

[15] D. Gordon and J. K. Udupa. Fast surface tracking in three-dimensional binary images. *Computer Vision, Graphics, and Image Processing*, 45(2):196–241, February 1989.

[16] G. T. Herman. Discrete Multidimensional Jordan Surfaces. *Computer Vision, Graphics, and Image Processing*, 54(6):507–515, November 1992.

[17] G. T. Herman. Finitary 1-simply connected digital spaces. *Graphical Models and Image Processing*, 60(1):46–56, January 1998.

[18] G.T. Herman. Oriented Surfaces in Digital Spaces. *CVGIP: Graphical Models and Image Processing*, 55(5):381–396, September 1993.

[19] G.T. Herman and D. Webster. A topological proof of a surface tracking algorithm. *Computer Vision, Graphics, and Image Processing*, 23:162–177, 1983.

[20] A.D. Kalvin, C.B. Cutting, B. Haddad, and M.E. Noz. Constructing Topologically Connected Surfaces for the Comprehensive Analysis of 3D Medical Structures. *Proc. of SPIE Medical Imaging V: Image Processing*, 1445:247–258, 1991.

[21] Y. Kenmochi, A. Imiya, and N.F. Ezquerra. Polyhedra Generation from Lattice Points. In *Proc. of 6th Discrete Geometry for Computer Imagery*, volume 1176 of *Lecture Notes in Computer Science*, pages 127–138, Lyon, France, 1996. Springer-Verlag.

[22] T. Y. Kong and A. Rosenfeld. Digital Topology: Introduction and Survey. *Computer Vision, Graphics, and Image Processing*, 48(3):357–393, December 1989.

[23] T.Y. Kong and A.W. Roscoe. Continuous Analogs of Axiomatized Digital Surfaces. *Computer Vision, Graphics, and Image Processing*, 29(1):60–86, January 1985.

[24] T.Y. Kong and J.K. Udupa. A justification of a fast surface tracking algorithm. *CVGIP: Graphical Models and Image Processing*, 54(6):507–515, November 1992.

[25] J.-O. Lachaud. Topologically Defined Iso-surfaces. Research Report 96-20, Laboratoire de l'Informatique du Parallélisme, ENS Lyon, France, 1996.

[26] J.-O. Lachaud. *Extraction de surfaces à partir d'images tridimensionnelles : approche discrète et approche par modèle déformable.* PhD thesis, Université Joseph Fourier, Grenoble, France, 1998. (en français).

[27] L. J. Latecki. 3D well-composed pictures. *Graphical Models and Image Processing*, 59(3):164–172, May 1997.

[28] S. Lefschetz. *Algebraic Topology*, volume XXVII of *Colloquium publications*. American Mathematical Society, New York, NY, 1942.

[29] H.K. Liu. Two and three dimensional boundary detection. *Computer Graphics and Image Processing*, 6(2):123–134, April 1977.

[30] W. E. Lorensen and H. E. Cline. Marching Cubes: A High Resolution 3D Surface Construction Algorithm. *Computer Graphics*, 21(4):163–169, July 1987.

[31] R. Malgouyres. *Une définition des surfaces de Z3*. PhD thesis, Université d'Auvergne, Clermont-Ferrand, France, February 1994.

[32] S. Miguet and L. Perroton. Discrete surfaces of 26-connected sets of voxels. In *Proc. of 5th Discrete Geometry for Computer Imagery*, Clermont-Ferrand, France, September 1995.

[33] D. G. Morgenthaler and A. Rosenfeld. Surfaces in Three-Dimensional Digital Images. *Information and Control*, 51(3):227–247, December 1981.

[34] H. Müller and M. Stark. Adaptive Generation of Surfaces in Volume Data. *The Visual Computer*, 9:182–199, 1993.

[35] B.K. Natarajan. On generating topologically consistent isosurfaces from uniform samples. *The Visual Computer*, 11(1):52–62, 1994.

[36] G.M. Nielsen and B. Hamman. The Asymptotic Decider: Resolving the Ambiguity in Marching Cubes. In *Proc. of IEEE Visualization'91*, pages 83–90, San Diego, USA, 1991.

[37] L. Perroton. A 26-connected object surface tracking algorithm. *Géométrie discrète en imagerie, fondements et applications*, 1:1–10, September 1993.

[38] S. Röll, A. Haase, and M. von Kienlin. Fast Generation of Leakproof Surfaces from Well-Defined Objects by a Modified Marching Cubes Algorithm. *Computer Graphics Forum*, 14(2):127–138, January 1995.

[39] A. Rosenfeld, T.Y. Kong, and A.Y. Wu. Digital Surfaces. *CVGIP: Graphical Models and Image Processing*, 53(4):305–312, July 1991.

[40] R. Shu, C. Zhou, and M.S. Kankanhalli. Adaptive marching cubes. *The Visual Computer*, 11(4):202–217, 1995.

[41] J. K. Udupa. Multidimensional Digital Boundaries. *CVGIP: Graphical Models and Image Processing*, 56(4):311–323, July 1994.

[42] J. K. Udupa and V. G. Ajjanagadde. Boundary and object labelling in three-dimensional images. *Computer Vision, Graphics, and Image Processing*, 51(3):355–369, September 1990.

[43] J.K. Udupa, H.M. Hung, and K.S. Chuang. Surface and Volume Rendering in Three-dimensional Imaging: A Comparison. *Journal of Digital Imaging*, 4(3):159–168, August 1991.

[44] J. Wilhelms and A. Van Gelder. Octrees for Faster Isosurface Generation. *ACM Transactions on Graphics*, 11(3):201–227, July 1992.

[45] G. Wyvill, C. McPheeters, and B. Wyvill. Data Structures for Soft Objects. *The Visual Computer*, 2(4):227–234, August 1986.

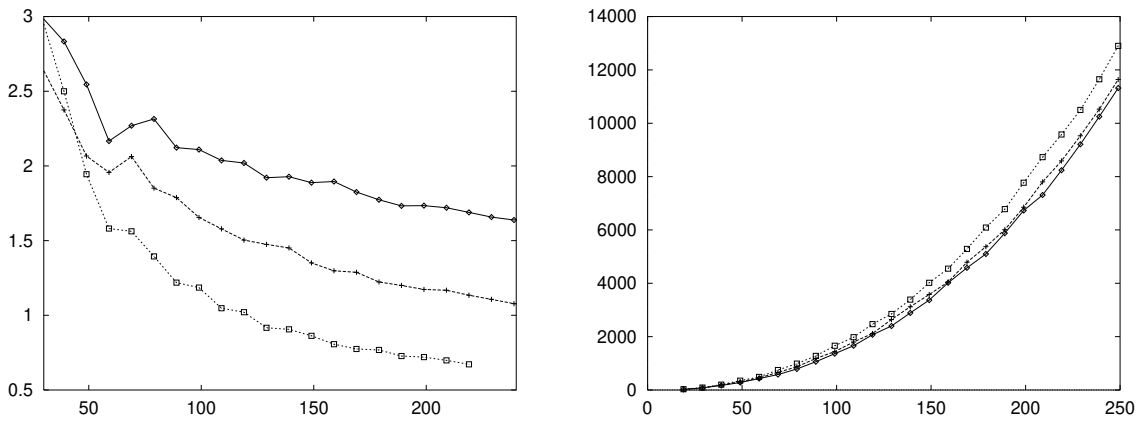

(a) (b)

Figure 9: This figure compares the performance of two approaches to extract the iso-surface: (1) the scanning approach and (2) the transformation of the digital boundary extracted by tracking. The test image is a sphere (images are cubical; the numbers in abscissa represent the side sizes of those images), constructed as a gray-level image, to which pepper and salt noise may be added. The phrase "p% of pepper and salt noise added to the image" means the gray intensity of every voxel has a p% probability to be set to either black or white. The graph with diamond points and solid lines designates the test image without noise. The graph with cross points and dashed lines indicates the test image with 1% of pepper and salt noise and the graph with square points and dotted lines the test image with 5% of noise. Graph (a) draws the time ratio between method (2) and method (1) as a function of the image side size. Graph (b) draws the computation time taken by method (2) as a function of the image side size (time in ms on a 300 Mhz Pentium PC).